Science Advances
AAAS

Supplementary Materials for

Evolutionary epigenomic analyses in mammalian early embryos reveal species-specific innovations and conserved principles of imprinting

Xukun Lu, Yu Zhang, Lijuan Wang, Leyun Wang, Huili Wang, Qianhua Xu, Yunlong Xiang, Chaolei Chen, Feng Kong, Weikun Xia, Zili Lin, Sinan Ma, Ling Liu, Xiangguo Wang, Hemin Ni, Wei Li*, Yong Guo*, Wei Xie*

*Corresponding author. Email: liwei@ioz.ac.cn (W.L.); y63guo@126.com (Y.G.); xiewei121@tsinghua.edu.cn (W.X.)

Published 24 November 2021, *Sci. Adv.* **7**, eabi6178 (2021)
DOI: 10.1126/sciadv.abi6178

The PDF file includes:

Other Supplementary Material for this manuscript includes the following:

Figure S1

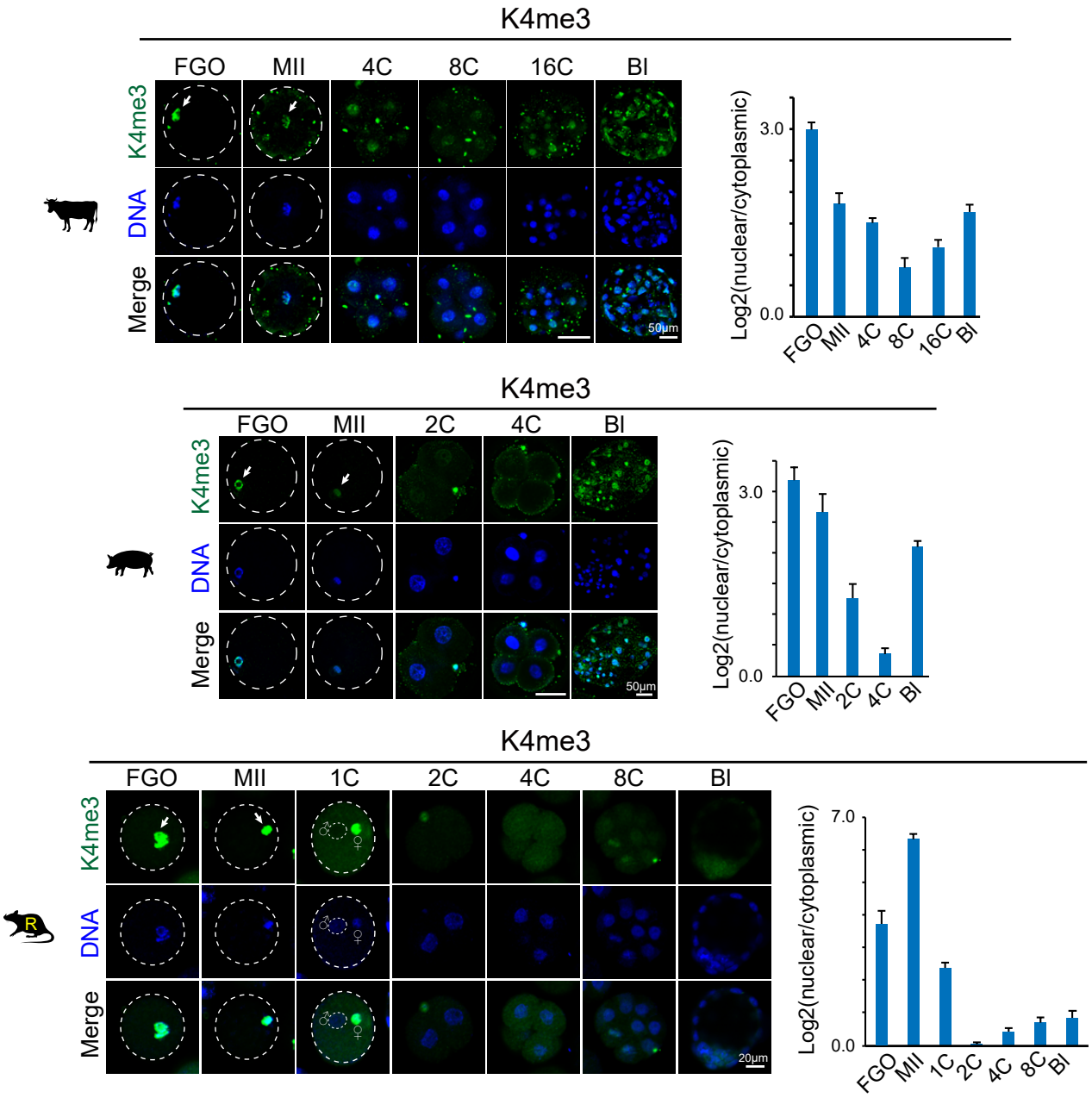

Figure S1. The dynamics of H3K4me3 in mammalian oocytes and preimplantation embryos. Immunofluorescent staining results showing the dynamics of H3K4me3 (K4me3) from FGO to blastocyst in bovine, porcine, and rat. The oocytes are circled by white dashed lines. White arrows indicate the nuclei and chromatin for FGOs and MII oocytes, respectively. In rat 1-cell, both female and male pronucleus (small white dashed lines) are shown. For bovine and porcine samples, bar=50 μm; for rat samples, bar=20 μm. The relative levels of H3K4me3 (log2 transformed nuclear/cytoplasmic fluorescence intensity, mean±SEM) at each stage of the three species are shown on the right. FGO, full-grown oocyte; MII, metaphase II-stage oocyte; 1C, 1-cell embryo; 2C, late 2-cell embryo; 4C, 4-cell embryo; 8C, 8-cell embryo; 16C, 16-cell embryo; Bl, blastocyst.

Figure S2

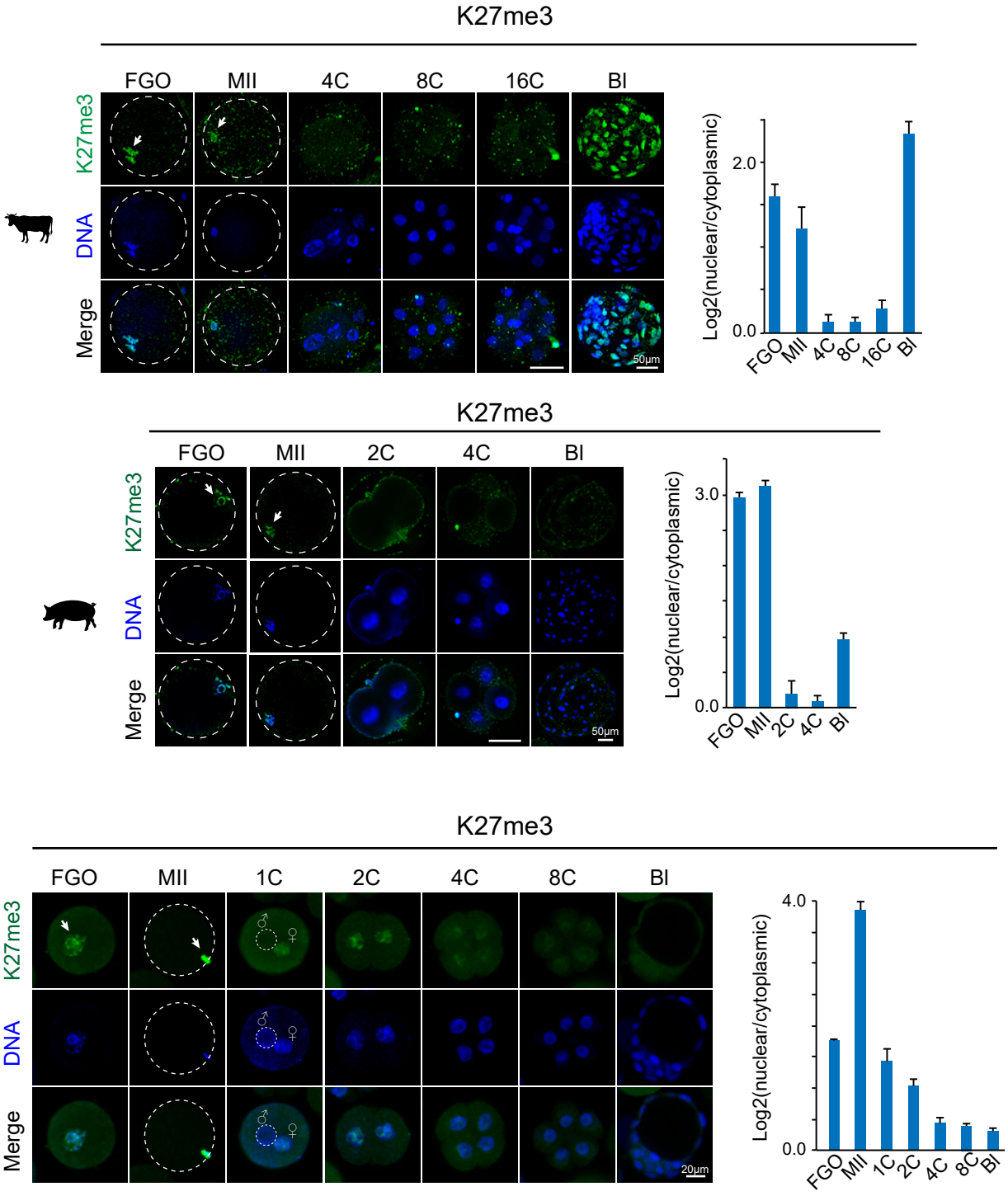
K27me3
FGO
MII
4C
8C
16C
BI
K27me3
DNA
Merge
50μm
Log2(nuclear/cytoplasmic)
2.0
0.0
FGO
MII
4C
8C
16C
BI
K27me3
FGO
MII
2C
4C
BI
K27me3
DNA
Merge
50μm
Log2(nuclear/cytoplasmic)
3.0
0.0
FGO
MII
2C
4C
BI
K27me3
FGO
MII
1C
2C
4C
8C
BI
K27me3
DNA
Merge
20μm
Log2(nuclear/cytoplasmic)
4.0
0.0
FGO
MII
1C
2C
4C
8C
BI

Figure S2. The dynamics of H3K27me3 in mammalian oocytes and preimplantation embryos. Immunofluorescent staining results showing the dynamics of H3K27me3 (K27me3) from FGO to blastocyst in bovine, porcine, and rat. The oocytes are circled by white dashed lines. White arrows indicate the nuclei or chromatins of FGOs or MII oocytes, respectively. In rat 1-cell, both female and male pronucleus (small white dashed lines) are shown. For bovine and porcine samples, bar=50 μm; for rat samples, bar=20 μm. The relative levels of H3K27me3 (log2 transformed nuclear/cytoplasmic fluorescence intensity) at each stage of the three species are shown on the right. Data are shown as mean±SEM. FGO, full-grown oocyte; MII, metaphase II-stage oocyte; 1C, 1-cell embryo; 2C, late 2-cell embryo; 4C, 4-cell embryo; 8C, 8-cell embryo; 16C, 16-cell embryo; Bl, blastocyst.

Figure S3

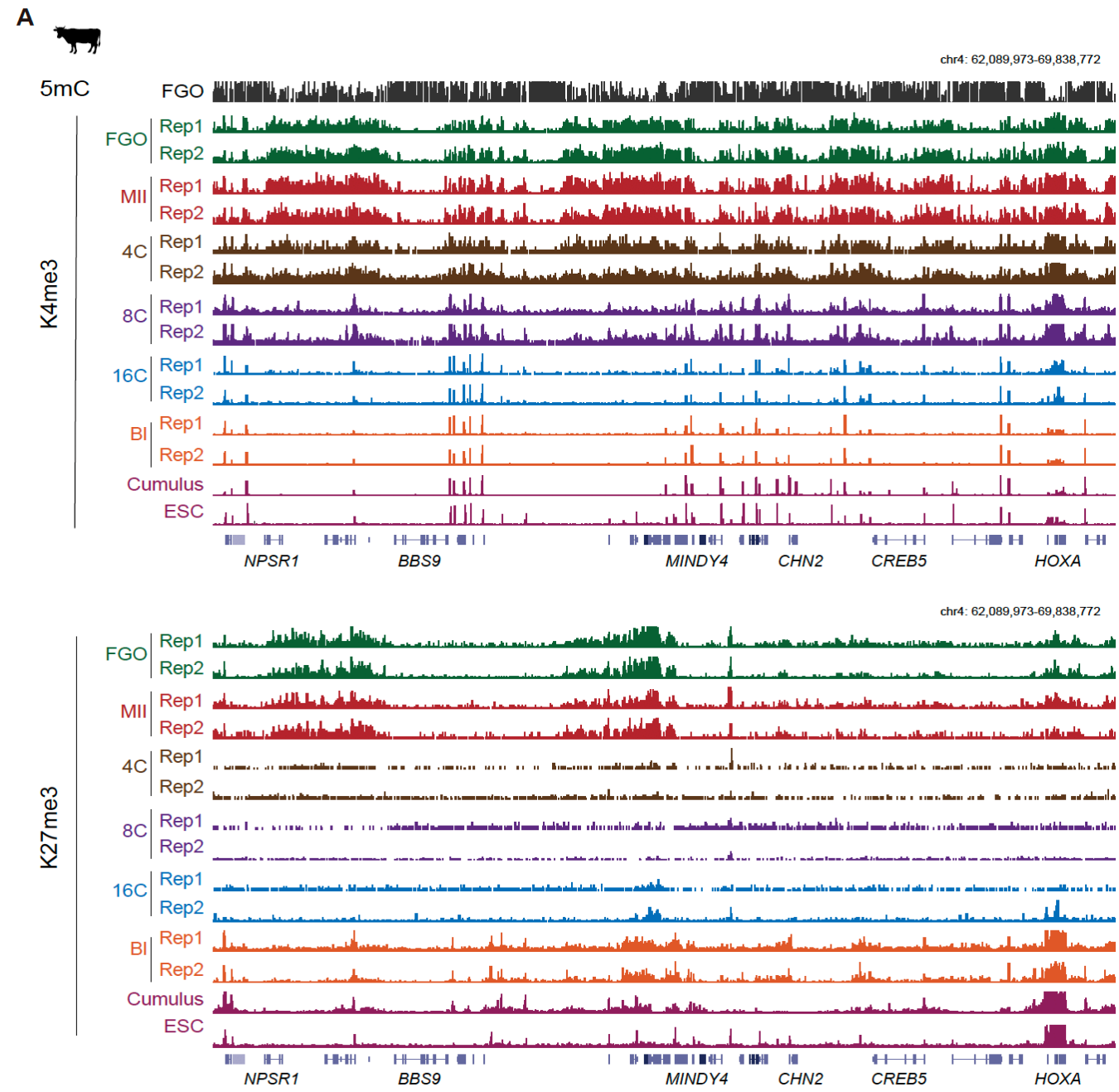
A
chr4: 62,089,973-69,838,772
5mC
FGO
K4me3
FGO
Rep1
Rep2
MII
Rep1
Rep2
4C
Rep1
Rep2
8C
Rep1
Rep2
16C
Rep1
Rep2
BI
Rep1
Rep2
Cumulus
ESC
NPSR1
BBS9
MINDY4
CHN2
CREB5
HOXA
chr4: 62,089,973-69,838,772
K27me3
FGO
Rep1
Rep2
MII
Rep1
Rep2
4C
Rep1
Rep2
8C
Rep1
Rep2
16C
Rep1
Rep2
BI
Rep1
Rep2
Cumulus
ESC
NPSR1
BBS9
MINDY4
CHN2
CREB5
HOXA
B
Correlation of replicates
K4me3
Correlation
1
0.5
0
FGO
MII
4C
8C
16C
BI
K27me3
Correlation
1
0.5
0
FGO
MII
4C
8C
16C
BI
Global loss

Figure S3. Global view of DNA methylation in FGOs and histone modifications in oocytes and early embryos in bovine. (**A**) UCSC genome browser views showing DNA methylation (5mC) in FGOs, two replicates of H3K4me3 (K4me3) and H3K27me3 (K27me3) in FGO, MII, 4C, 8C, 16C and Bl. Cumulus cell and ESC data (*69*) are also shown for comparison. (**B**) Barplots showing the Pearson correlation between replicates for H3K4me3 and H3K27me3 data in bovine. FGO, full-grown oocyte; MII, metaphase II-stage oocyte; 4C, 4-cell embryo; 8C, 8-cell embryo; 16C, 16-cell embryo; Bl, blastocyst. Note the stages showing lower correlation are those when H3K27me3 undergoes global loss (indicated).

Figure S4

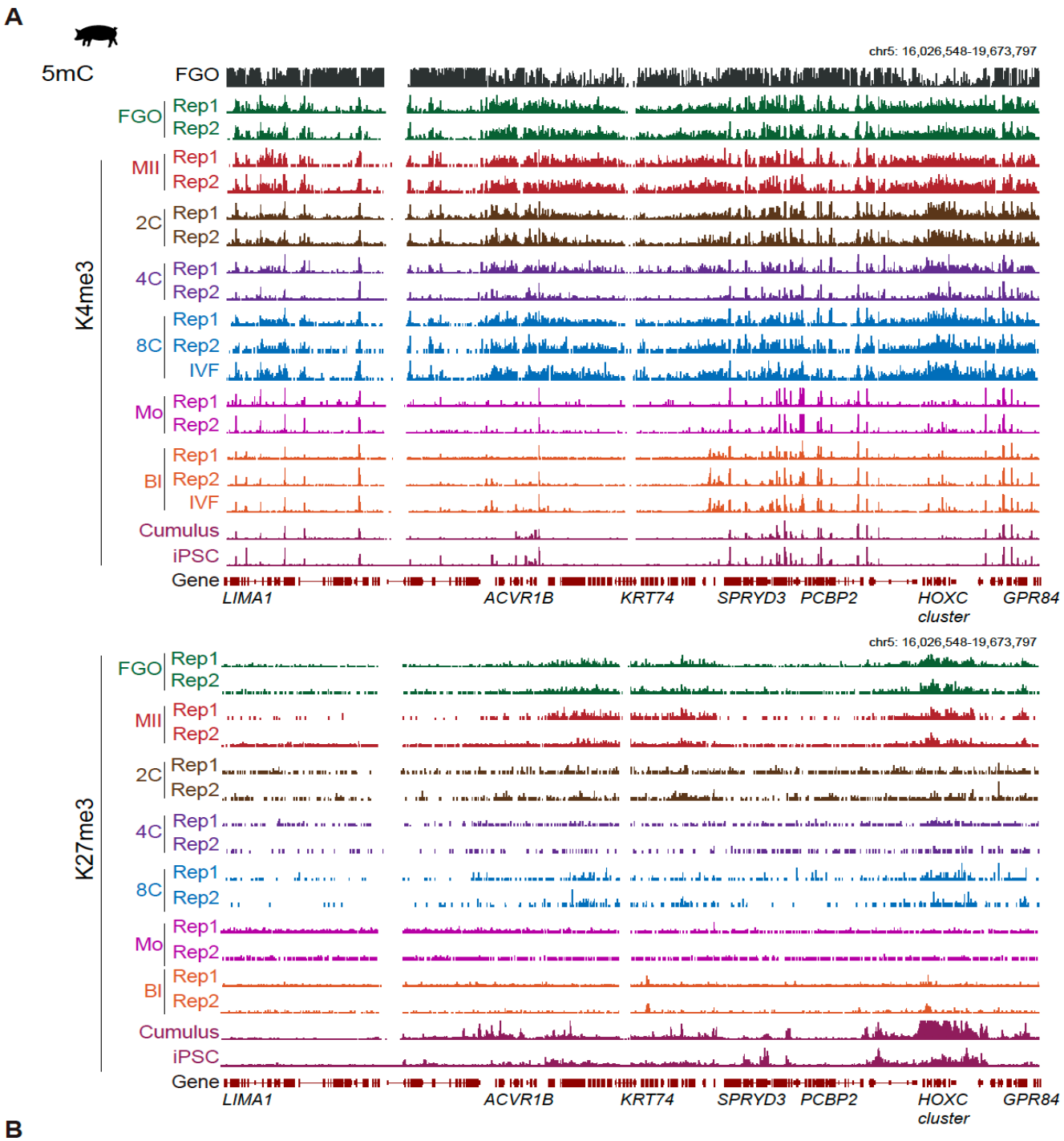
A
5mC
chr5: 16,026,548-19,673,797
FGO
FGO Rep1
FGO Rep2
MII Rep1
MII Rep2
2C Rep1
2C Rep2
4C Rep1
4C Rep2
8C Rep1
8C Rep2
8C IVF
Mo Rep1
Mo Rep2
Bl Rep1
Bl Rep2
Bl IVF
Cumulus
iPSC
Gene
K4me3
LIMA1
ACVR1B
KRT74
SPRYD3
PCBP2
HOXC cluster
GPR84
chr5: 16,026,548-19,673,797
K27me3
B
Correlation of replicates
K4me3
K27me3
Correlation
1
0.5
0
FGO
MII
2C
4C
8C
Mo
Bl
Global loss

Figure S4. Global view of DNA methylation in FGOs and histone modifications in oocytes and early embryos in porcine. (**A**) UCSC genome browser views showing DNA methylation (5mC) in FGOs, two replicates of H3K4me3 (K4me3) and H3K27me3 (K27me3) in FGO, MII, 2C, 4C, 8C, Mo and Bl. Cumulus cell and iPSC data (*70*) are also shown for comparison. H3K4me3 in *in vitro* fertilized (IVF) 8C and blastocyst are also shown. (**B**) Barplots showing the Pearson correlation between replicates for H3K4me3 and H3K27me3 data in porcine. FGO, full-grown oocyte; MII, metaphase II-stage oocyte; 2C, late 2-cell embryo; 4C, 4-cell embryo; 8C, 8-cell embryo; Mo, morula, Bl, blastocyst. Note the stages showing lower correlation are those when H3K27me3 undergoes global loss (indicated).

Figure S5

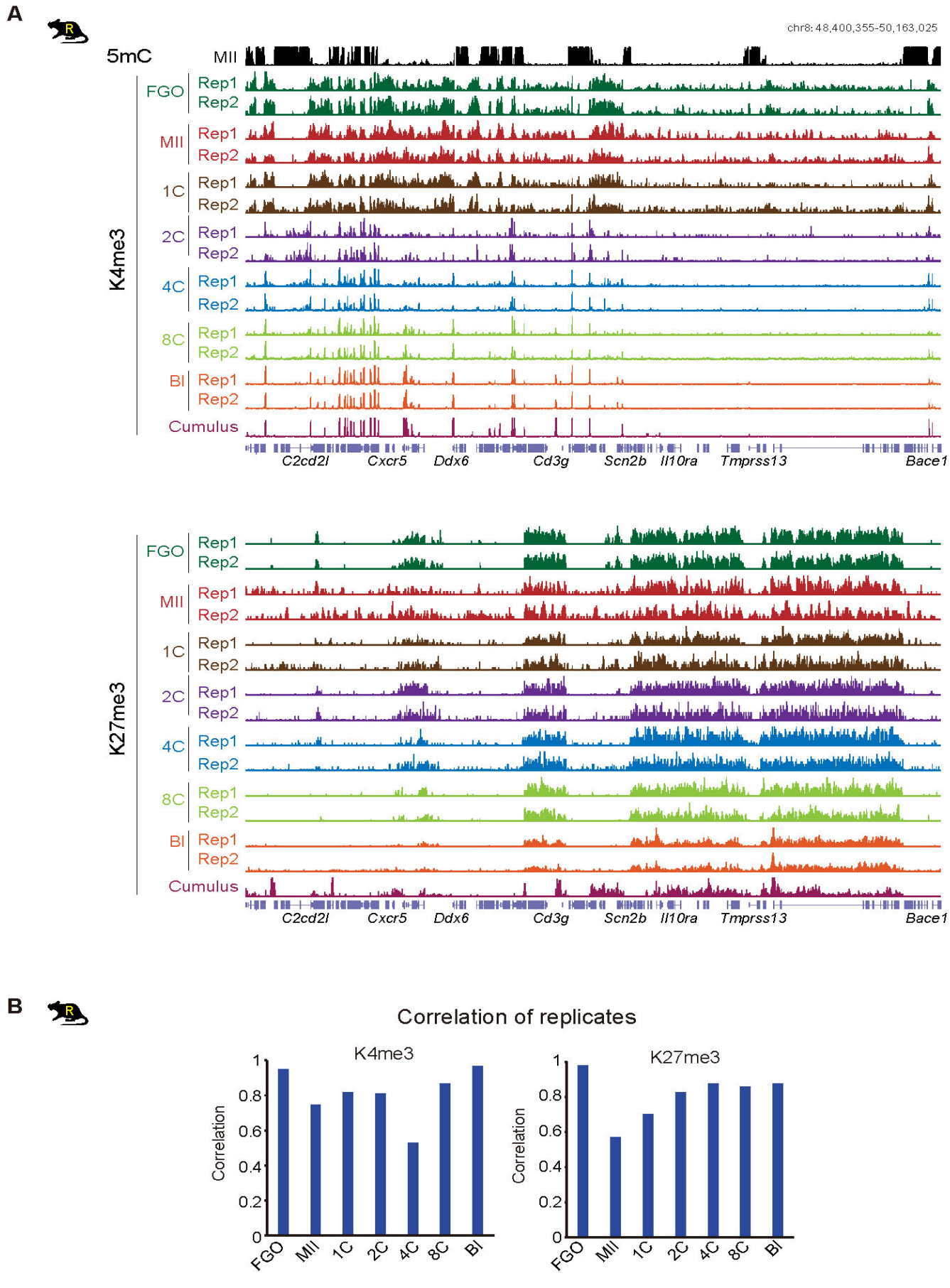
A
chr8: 48,400,355-50,163,025
5mC
MII
K4me3
FGO
MII
1C
2C
4C
8C
BI
Cumulus
Rep1
Rep2
C2cd2l
Cxcr5
Ddx6
Cd3g
Scn2b
Il10ra
Tmprss13
Bace1
K27me3
B
Correlation of replicates
K4me3
K27me3
Correlation
FGO
MII
1C
2C
4C
8C
BI

Figure S5. Global view of DNA methylation in MII oocytes and histone modifications in oocytes and early embryos in rat. (**A**) UCSC genome browser views showing DNA methylation (5mC) in MII oocytes (*26*), two replicates of H3K4me3 (K4me3) and H3K27me3 (K27me3) in FGO, MII, 1C, 2C, 4C, 8C and Bl. Cumulus cell data are also shown for comparison. (**B**) Barplots showing the Pearson correlation between replicates for H3K4me3 and H3K27me3 data in rat. FGO, full-grown oocyte; MII, metaphase II-stage oocyte; 1C, 1-cell embryo; 2C, late 2-cell embryo; 4C, 4-cell embryo; 8C, 8-cell embryo; Bl, blastocyst.

Figure S6

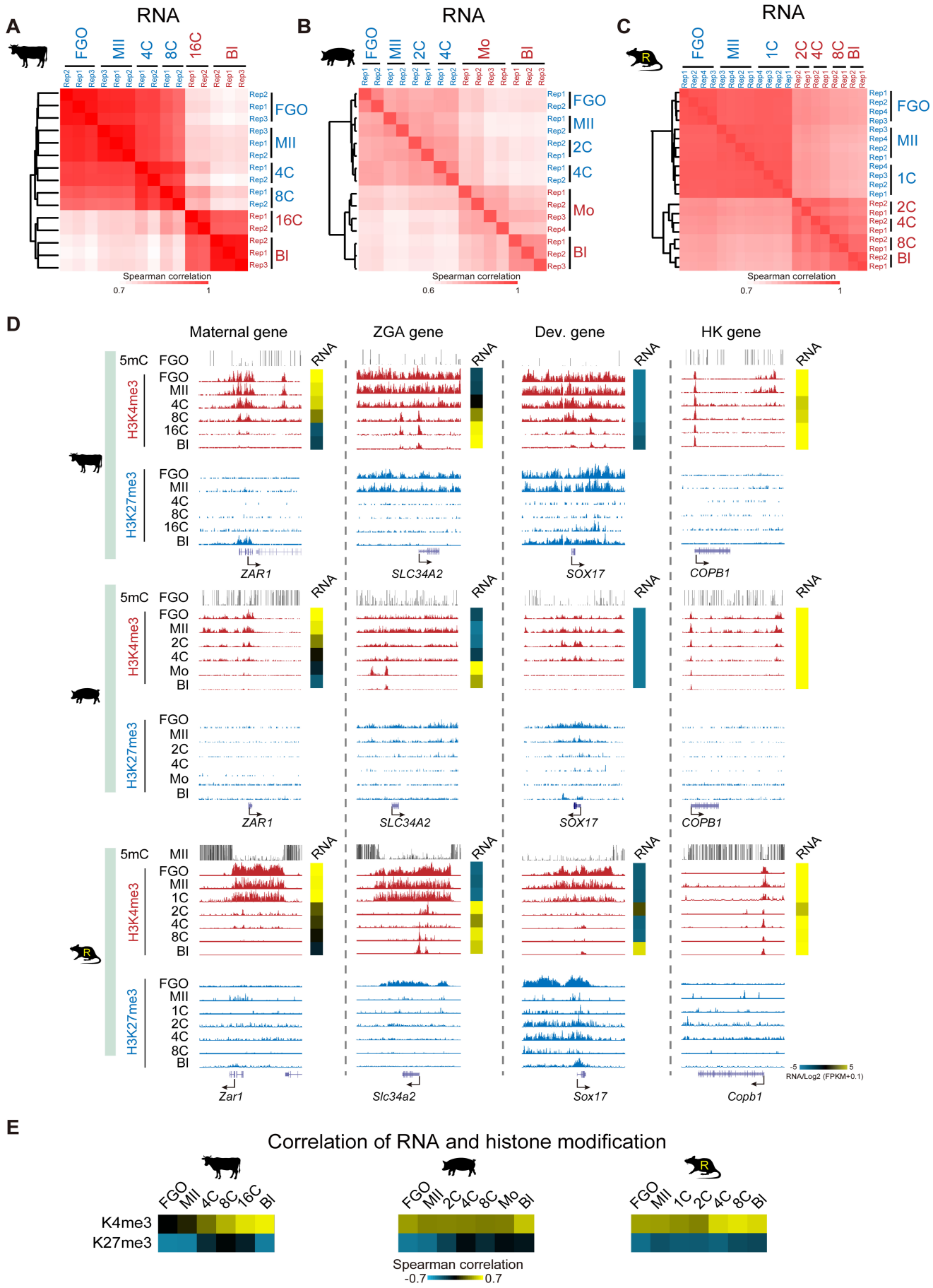
A
RNA
FGO
MII
4C
8C
16C
BI
Spearman correlation
0.7
1
B
RNA
FGO
MII
2C
4C
Mo
BI
Spearman correlation
0.6
1
C
RNA
FGO
MII
1C
2C
4C
8C
BI
Spearman correlation
0.7
1
D
Maternal gene
ZGA gene
Dev. gene
HK gene
5mC
H3K4me3
H3K27me3
RNA
ZAR1
SLC34A2
SOX17
COPB1
Zar1
Slc34a2
Sox17
Copb1
RNA/Log2 (FPKM+0.1)
E
Correlation of RNA and histone modification
K4me3
K27me3
Spearman correlation
-0.7
0.7

Figure S6. Global view of RNA-seq data in mammalian oocytes and early embryos. (**A**) Heatmap showing the pairwise Spearman correlation between replicates of the RNA-seq data among all development stages in bovine. The cluster on the left shows the relationship of all development stages. Blue, the oocyte and pre-ZGA stages; red, the post-ZGA stages. (**B** and **C**) Similar analysis as **a** for porcine (**B**) and rat (**C**). (**D**) Snapshots from UCSC genome browser showing the distribution of DNA methylation (5mC), H3K4me3 (K4me3) and H3K27me3 (K27me3) signals at representative gene loci in the oocytes and pre-implantation embryos of bovine, porcine and rat. Gene expression is also shown by heatmaps (log2 transformed FPKM+0.1). ZGA, zygotic genome activation; Dev., developmental; HK, housekeeping gene. (**E**) Heatmaps showing the Spearman correlation between promoter H3K4me3 (K4me3) or H3K27me3 (K27me3) and gene expression across all genes. FGO, full-grown oocyte; MII, metaphase II-stage oocyte; 1C, 1-cell embryo; 2C, late 2-cell embryo; 4C, 4-cell embryo; 8C, 8-cell embryo; 16C, 16-cell embryo; Mo, morula; Bl, blastocyst; ICM, inner cell mass.

Figure S7

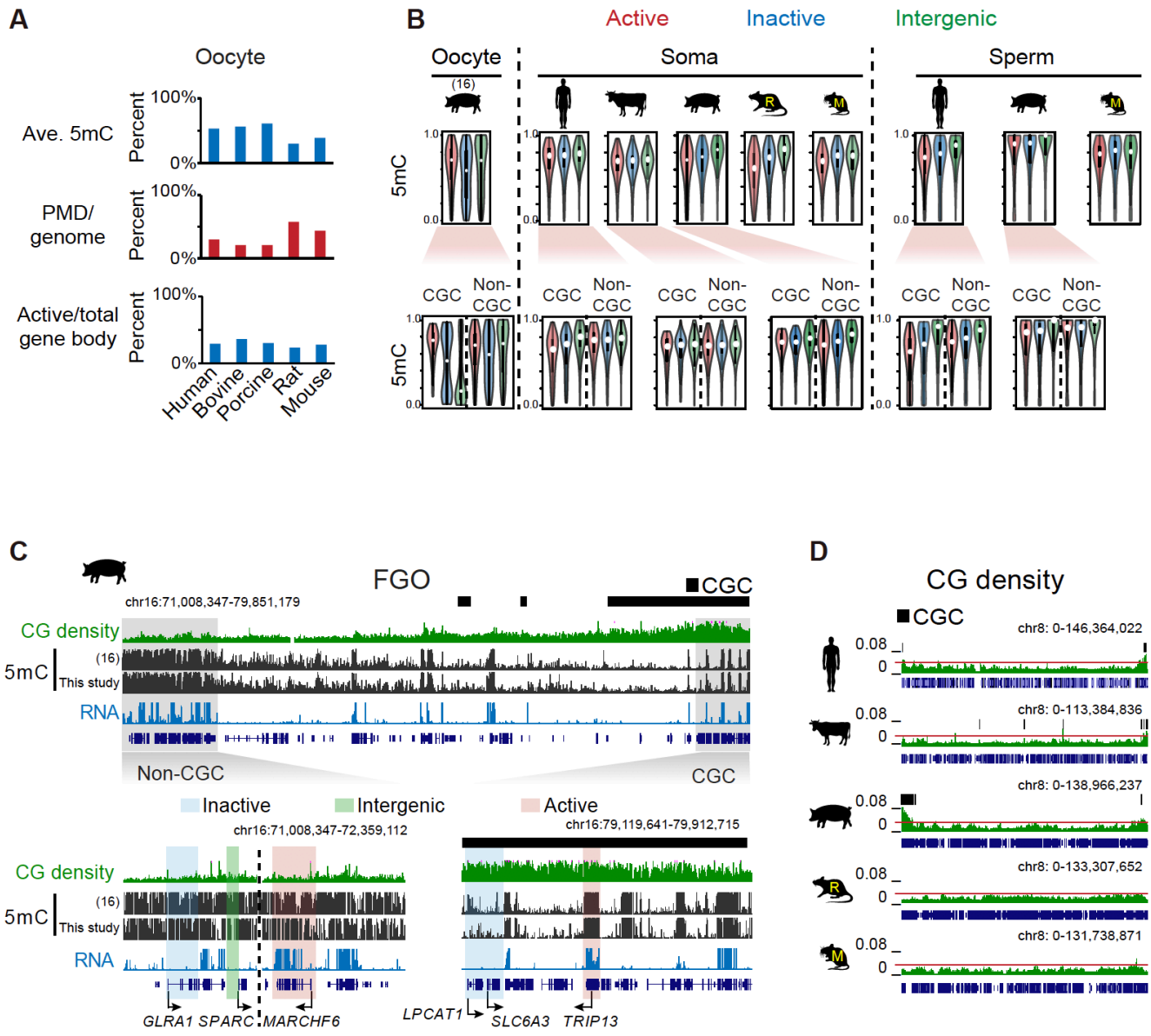

Figure S7. DNA methylation and CpG continents (CGCs) in mammalian oocytes. (**A**) Barplots showing the global DNA methylation (5mC) levels (top), PMD coverages (middle) and the percentages of active/total gene body (bottom) in the oocytes of human, bovine, porcine, rat and mouse. (**B**) Top, violin plots showing the DNA methylation levels in active gene bodies (red), inactive gene bodies (blue), and intergenic regions (green) in porcine oocytes, somatic tissues (Soma) in the five species, and sperm in human, porcine and mouse. Bottom, similar analyses were conducted for CGC and non-CGC regions in corresponding tissues/cells (top) in human, bovine and porcine. Data resources used in this analysis: porcine MII oocytes (*16*); human liver (*73*); bovine lung (*74*); rat left ventricle (*75*); mouse cerebellum (*76*); human sperm (*24*); porcine sperm (*16*); mouse sperm (*81*). (**C**) The UCSC genome browser views showing DNA methylation states in CGC (right) and non-CGC (left) regions in porcine FGOs. Active gene bodies, inactive gene bodies and intergenic regions are shaded. Data from (*16*) are included as a positive control. (**D**) The UCSC genome browser views showing the CG density across the entire chromosome (chr8) among the five species. CGCs are shown. The red line indicates the cutoff (0.03) for CGCs.

Figure S8

A

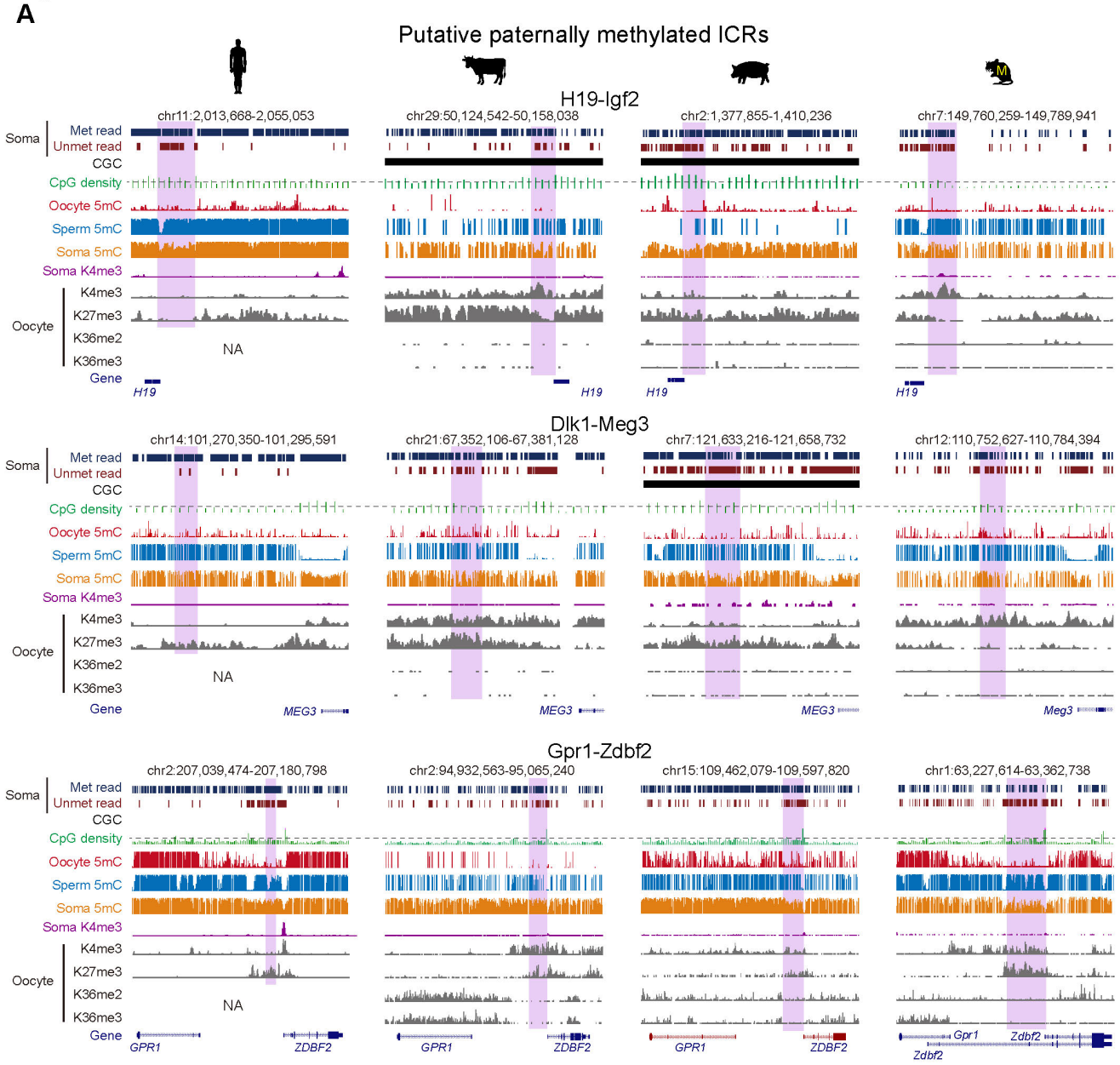
Putative paternally methylated ICRs
H19-Igf2
chr11:2,013,668-2,055,053
chr29:50,124,542-50,158,038
chr2:1,377,855-1,410,236
chr7:149,760,259-149,789,941
Soma
Met read
Unmet read
CGC
CpG density
Oocyte 5mC
Sperm 5mC
Soma 5mC
Soma K4me3
Oocyte
K4me3
K27me3
K36me2
K36me3
NA
Gene
H19
Dlk1-Meg3
chr14:101,270,350-101,295,591
chr21:67,352,106-67,381,128
chr7:121,633,216-121,658,732
chr12:110,752,627-110,784,394
MEG3
Meg3
Gpr1-Zdbf2
chr2:207,039,474-207,180,798
chr2:94,932,563-95,065,240
chr15:109,462,079-109,597,820
chr1:63,227,614-63,362,738
GPR1
ZDBF2
Gpr1
Zdbf2

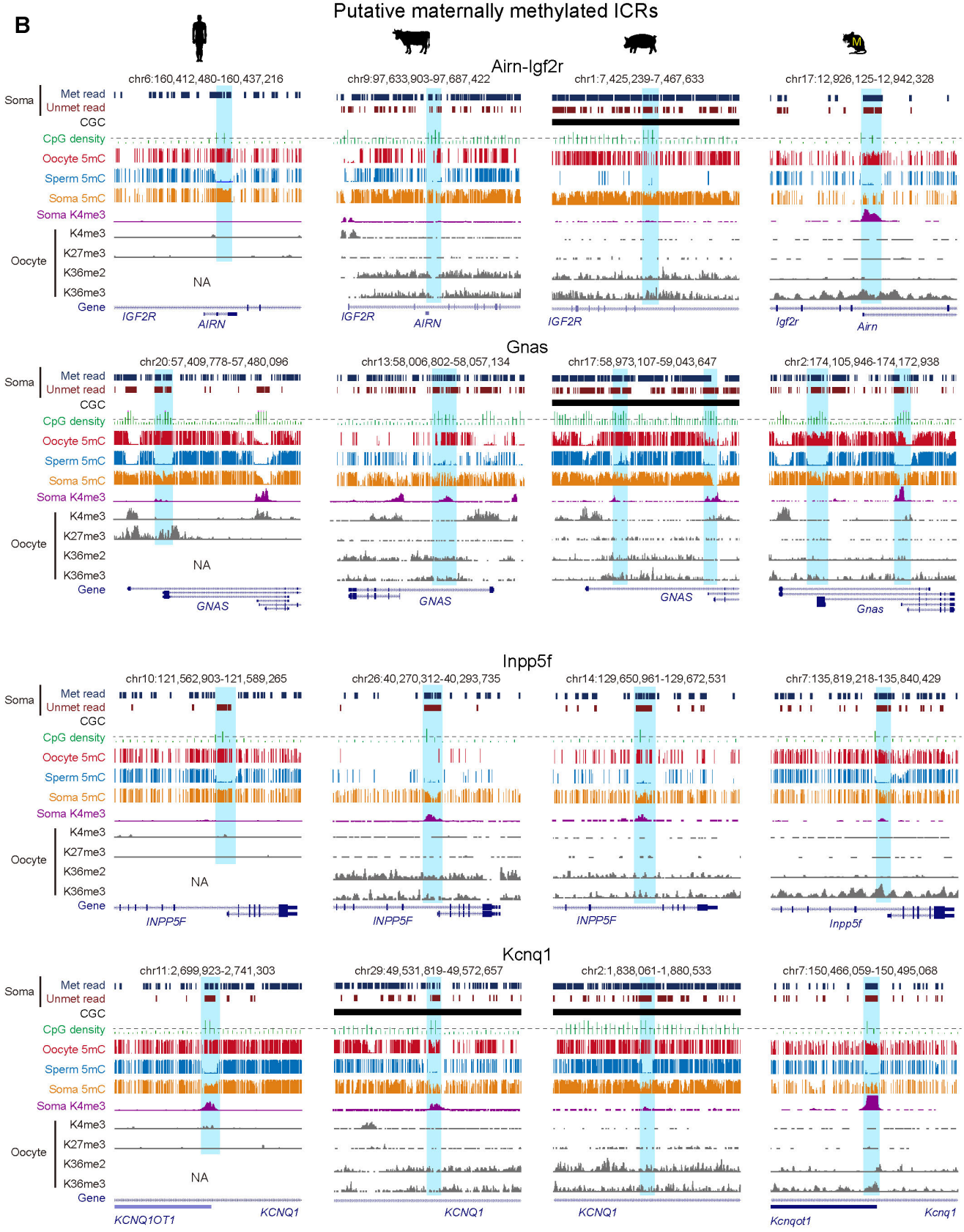
B
Putative maternally methylated ICRs
Airn-Igf2r
chr6:160,412,480-160,437,216
chr9:97,633,903-97,687,422
chr1:7,425,239-7,467,633
chr17:12,926,125-12,942,328
Gnas
chr20:57,409,778-57,480,096
chr13:58,006,802-58,057,134
chr17:58,973,107-59,043,647
chr2:174,105,946-174,172,938
Inpp5f
chr10:121,562,903-121,589,265
chr26:40,270,312-40,293,735
chr14:129,650,961-129,672,531
chr7:135,819,218-135,840,429
Kcnq1
chr11:2,699,923-2,741,303
chr29:49,531,819-49,572,657
chr2:1,838,061-1,880,533
chr7:150,466,059-150,495,068
Soma
Met read
Unmet read
CGC
CpG density
Oocyte 5mC
Sperm 5mC
Soma 5mC
Soma K4me3
Oocyte
K4me3
K27me3
K36me2
K36me3
NA
Gene
IGF2R
AIRN
Igf2r
Airn
GNAS
Gnas
INPP5F
Inpp5f
KCNQ1OT1
KCNQ1
Kcnqot1
Kcnq1

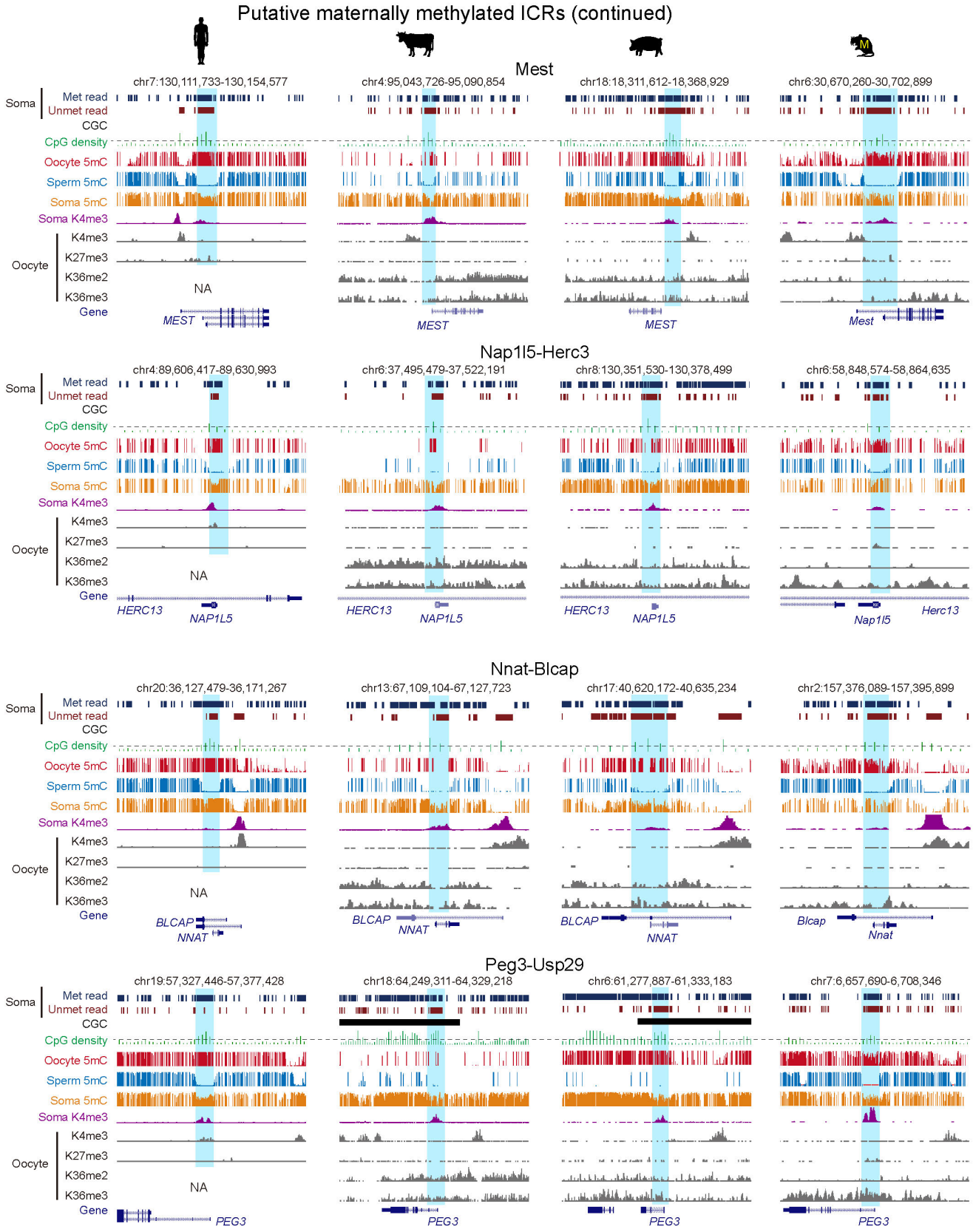
Putative maternally methylated ICRs (continued)
Mest
chr7:130,111,733-130,154,577
chr4:95,043,726-95,090,854
chr18:18,311,612-18,368,929
chr6:30,670,260-30,702,899
Soma
Met read
Unmet read
CGC
CpG density
Oocyte 5mC
Sperm 5mC
Soma 5mC
Soma K4me3
Oocyte
K4me3
K27me3
K36me2
K36me3
NA
Gene
MEST
MEST
MEST
Mest
Nap1l5-Herc3
chr4:89,606,417-89,630,993
chr6:37,495,479-37,522,191
chr8:130,351,530-130,378,499
chr6:58,848,574-58,864,635
HERC13
NAP1L5
HERC13
NAP1L5
HERC13
NAP1L5
Nap1l5
Herc13
Nnat-Blcap
chr20:36,127,479-36,171,267
chr13:67,109,104-67,127,723
chr17:40,620,172-40,635,234
chr2:157,376,089-157,395,899
BLCAP
NNAT
BLCAP
NNAT
BLCAP
NNAT
Blcap
Nnat
Peg3-Usp29
chr19:57,327,446-57,377,428
chr18:64,249,311-64,329,218
chr6:61,277,887-61,333,183
chr7:6,657,690-6,708,346
PEG3
PEG3
PEG3
PEG3

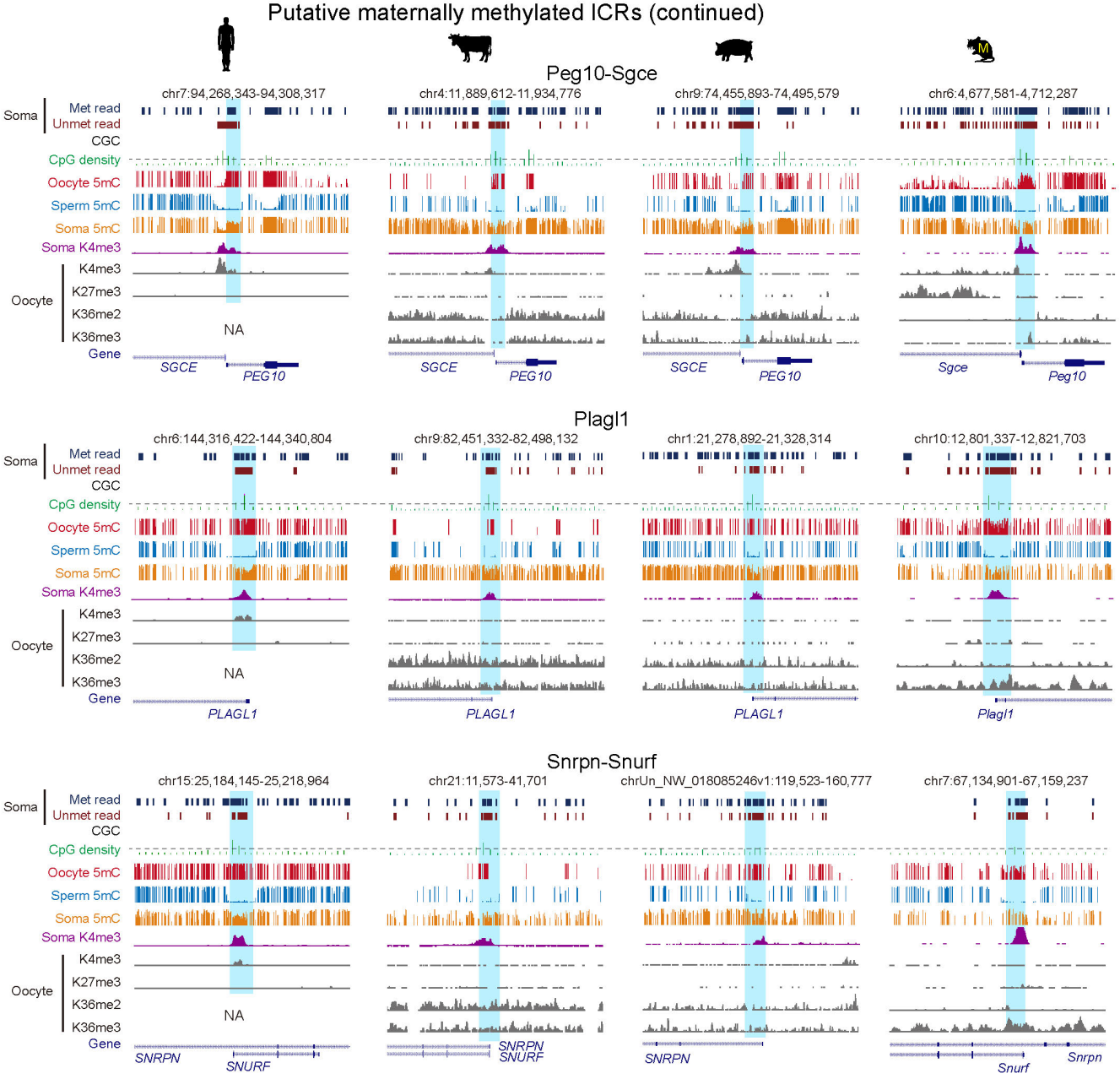
Putative maternally methylated ICRs (continued)
Peg10-Sgce
chr7:94,268,343-94,308,317
chr4:11,889,612-11,934,776
chr9:74,455,893-74,495,579
chr6:4,677,581-4,712,287
Soma
Met read
Unmet read
CGC
CpG density
Oocyte 5mC
Sperm 5mC
Soma 5mC
Soma K4me3
Oocyte
K4me3
K27me3
K36me2
K36me3
NA
Gene
SGCE
PEG10
Sgce
Peg10
Plagl1
chr6:144,316,422-144,340,804
chr9:82,451,332-82,498,132
chr1:21,278,892-21,328,314
chr10:12,801,337-12,821,703
PLAGL1
Plagl1
Snrpn-Snurf
chr15:25,184,145-25,218,964
chr21:11,573-41,701
chrUn_NW_018085246v1:119,523-160,777
chr7:67,134,901-67,159,237
SNRPN
SNURF
Snurf
Snrpn

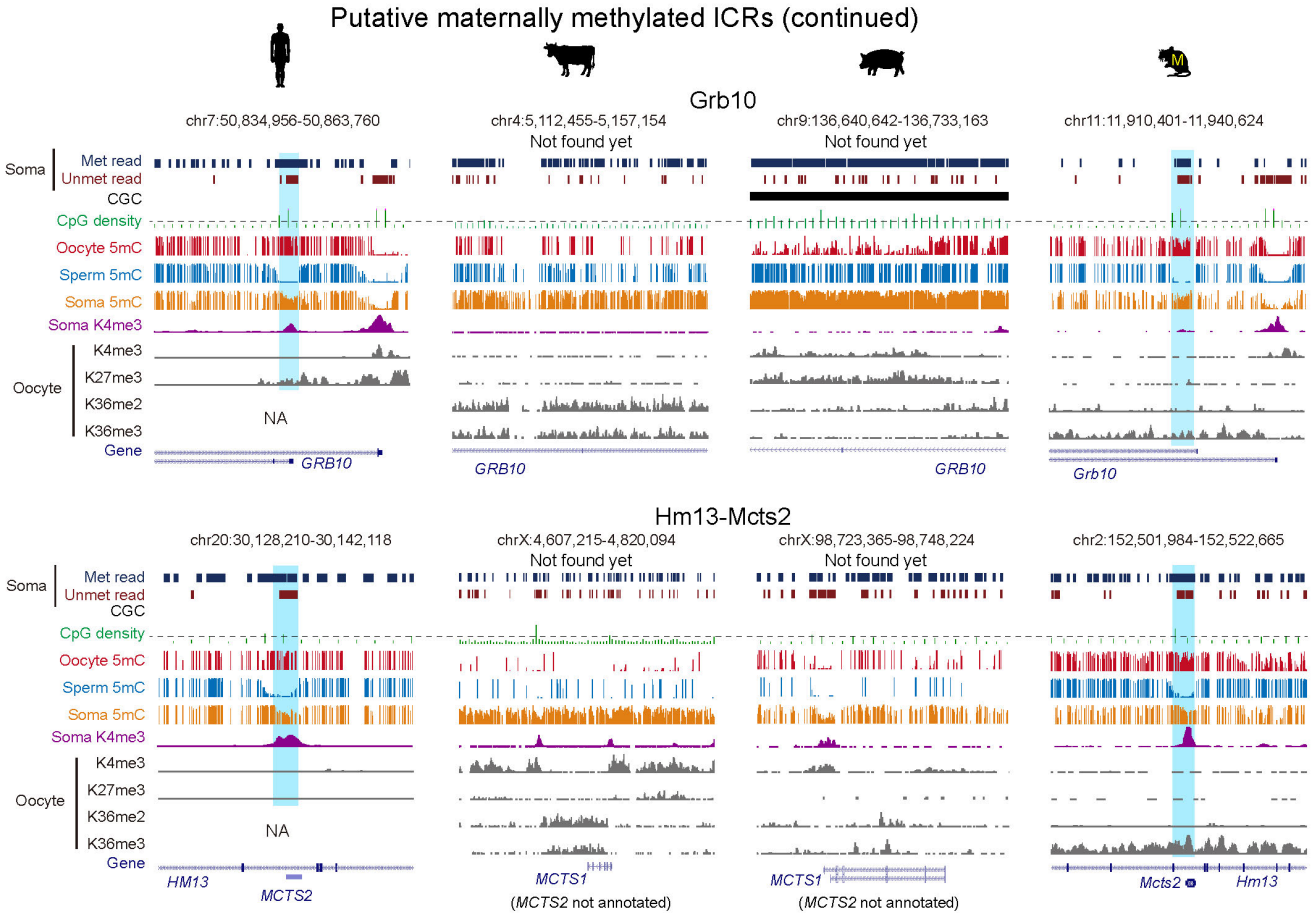

Figure S8. The putative paternal and maternal ICRs and their relationship with CGCs in bovine and porcine. The UCSC genome browser view showing the putative paternal (**A**, shaded in purple) and maternal (**B**, shaded in light blue) ICRs in bovine and porcine. Only germline ICRs conserved in mouse and human were considered. ICR positions for human and mouse were obtained from previous studies and related data were independently processed in this study (*24, 35*). The *GRB10* and *HM13-MCTS2* ICRs in bovine and porcine were not found yet. Only MCTS1, but not MCTS2, is annotated and is shown in bovine and porcine. CGC, CpG density (1 kb bin), DNA methylation (5mC) in oocyte, sperm and somatic tissues (Soma) (human: liver (*73*); bovine: lung (*74*); porcine: muscle (*78*); mouse: liver (*76*)), H3K4me3 (K4me3), H3K27me3 (K27me3), H3K36me2 (K36me2) and H3K36me3 (K36me3) in oocyte around these ICRs are shown. The dashed lines for CG density indicate the cutoff of 0.03 (100 kb bin) used for calling CGCs. Met read, reads with all CpGs (at least 3) methylated; Unmet read, reads with all CpGs (at least 3) unmethylated (human: liver; bovine: lung; porcine: muscle; mouse: liver).

Figure S9

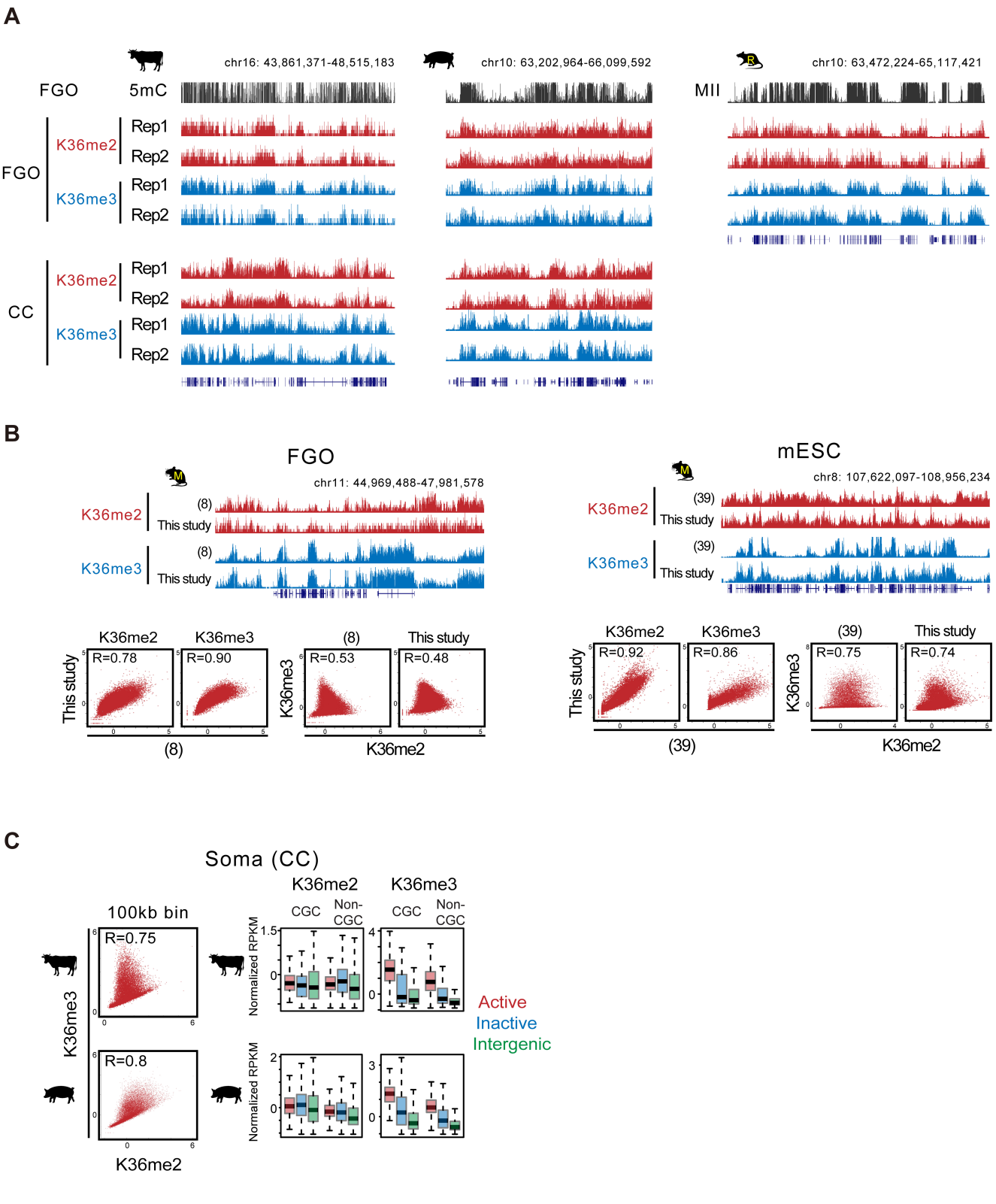
A
chr16: 43,861,371-48,515,183
chr10: 63,202,964-66,099,592
chr10: 63,472,224-65,117,421
FGO
5mC
MII
FGO
K36me2
K36me3
Rep1
Rep2
CC
B
FGO
mESC
chr11: 44,969,488-47,981,578
chr8: 107,622,097-108,956,234
(8)
(39)
This study
R=0.78
R=0.90
R=0.53
R=0.48
R=0.92
R=0.86
R=0.75
R=0.74
C
Soma (CC)
100kb bin
R=0.75
R=0.8
CGC
Non-CGC
Normalized RPKM
Active
Inactive
Intergenic

Figure S9. H3K36me2 and H3K36me3 in the oocytes and somatic cumulus cells (CCs) across mammals. (**A**) UCSC genome browser views showing DNA methylation (5mC) in oocytes, two replicates of H3K36me2 (K36me2) and H3K36me3 (K36me3) in FGOs of bovine, porcine and rat. H3K36me2 and H3K36me3 in cumulus cells (CCs) for bovine and porcine are also shown. (**B**) The UCSC genome browser views (top) and scatterplots (bottom) showing the comparison of H3K36me2 and H3K36me3 patterns in mouse FGOs in this study and a previous study (*8*), or in mESCs in this study and a previous study (*39*). Scatterplots comparing H3K36me2 and H3K36me3 from the same study are also shown. Data from previous studies were downloaded and processed independently in this study. (**C**) Scatterplots comparing H3K36me2 and H3K36me3 in CCs for bovine and porcine (left). Boxplots showing the enrichment of H3K36me2 and H3K36me3 in active gene bodies (red), inactive gene bodies (blue), and intergenic regions (green) in CGCs and non-CGCs in CCs for bovine and porcine.

Figure S10

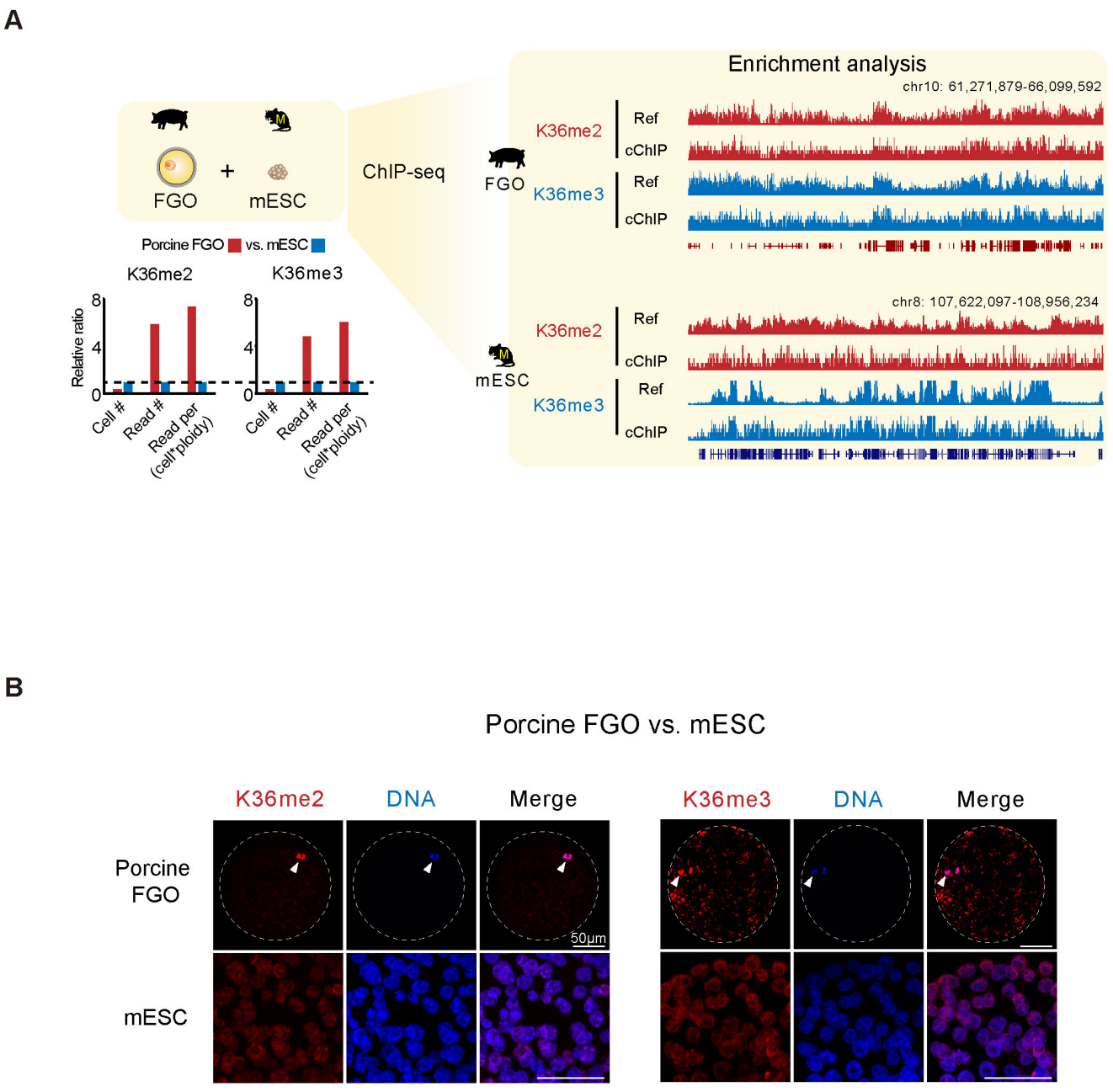

Figure S10. Validation of H3K36me2 and H3K36me3 in porcine oocytes. (**A**) Competitive and calibrated ChIP-seq (cChIP) result of H3K36me2 (K36me2) and H3K36me3 (K36me3) for porcine FGOs, with mESCs as references. A total of 100 FGOs (2n, 4C) and 250 mESCs (2n, 2C) were mixed and subjected to STAR ChIP-seq for H3K36me2 and H3K36me3. Sequencing reads were mapped separately to mouse and porcine genomes. Barplots showing the comparison of cell numbers, read numbers, read per (cell number*ploidy) between porcine FGOs and mESCs (set as 1). UCSC genome browser views (right) showing the comparison of H3K36me2 and H3K36me3 patterns in porcine FGOs and mESCs obtained from pure samples (Ref) or mixed samples (cChIP). (**B**) Immunofluorescent staining showing the abundance of H3K36me2 and H3K36me3 in porcine FGOs and mESCs. The oocytes are circled by white dashed lines. White arrows indicate the nuclei of porcine FGOs. Bar=50 μm.

Figure S11

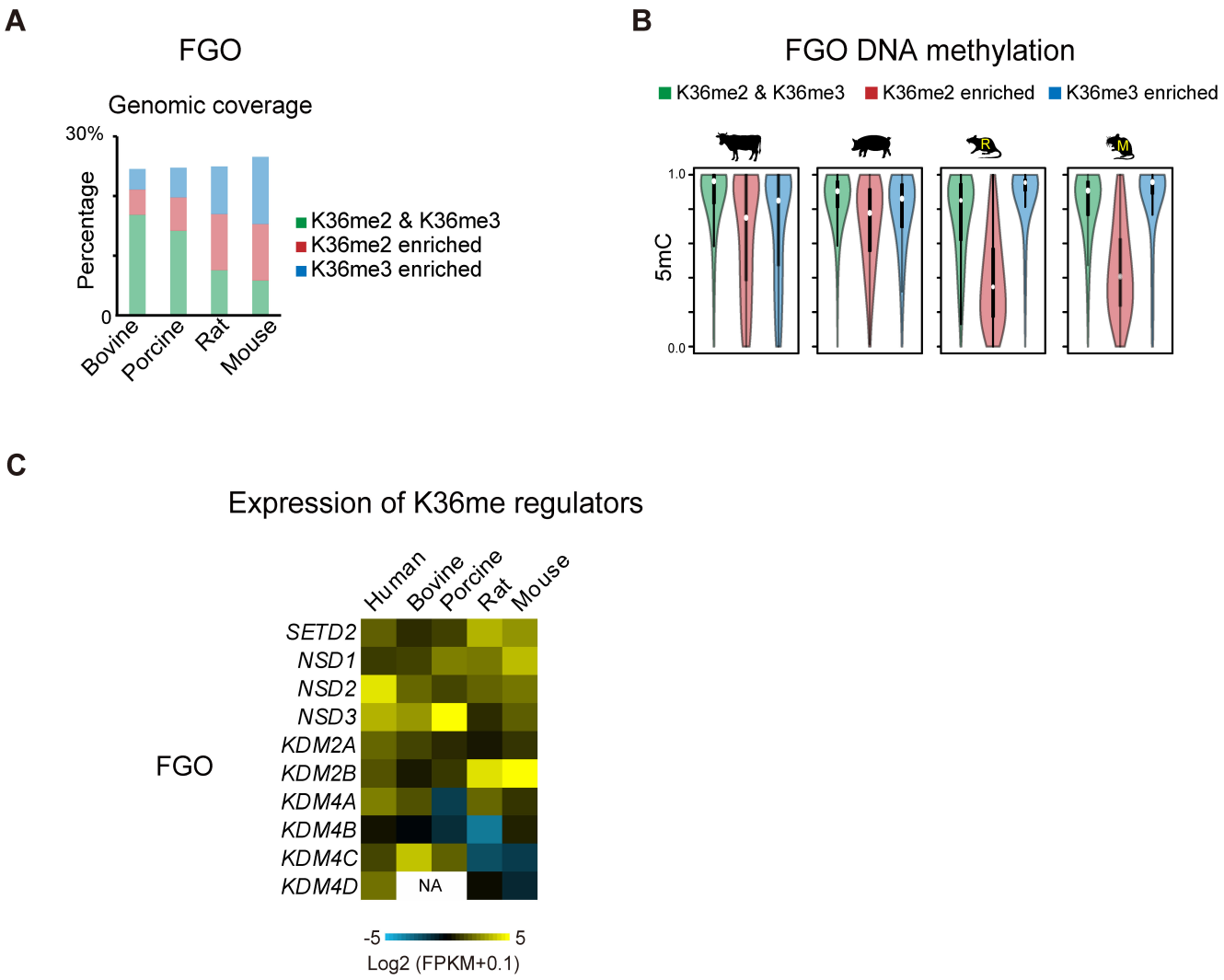

Figure S11. H3K36me2- and H3K36me3-correlated DNA methylation in the oocytes across mammals. (**A**) Barplot showing the percentages of the genome enriched by H3K36me2 (red), H3K36me3 (blue) or both H3K36me2 and H3K36me3 (green) in the oocytes of different species. (**B**) Violin plots showing the DNA methylation levels at regions enriched by H3K36me2 (K36me2 enriched, red), H3K36me3 (K36me3 enriched, blue) or both H3K36me2 and H3K36me3 (K36me2 & K36me3, green) in the oocytes across mammals. (**C**) Heatmap showing the expression of H3K36me2/3 regulators in the oocytes across the five species.

Figure S12

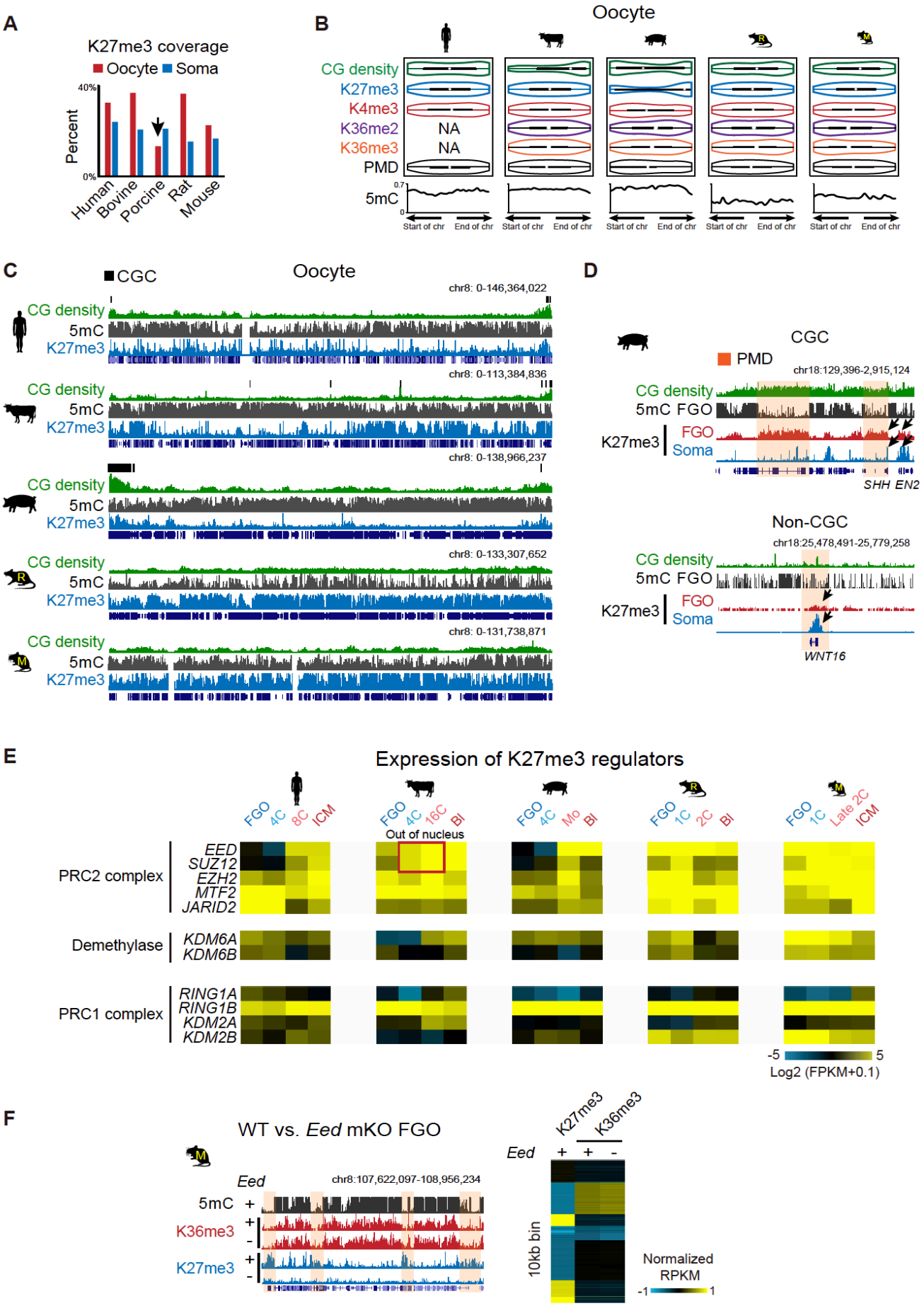
A
K27me3 coverage
Oocyte
Soma
40%
0%
Percent
Human
Bovine
Porcine
Rat
Mouse
B
Oocyte
CG density
K27me3
K4me3
K36me2
K36me3
PMD
NA
NA
5mC
0.7
0
Start of chr
End of chr
C
CGC
Oocyte
chr8: 0-146,364,022
chr8: 0-113,384,836
chr8: 0-138,966,237
chr8: 0-133,307,652
chr8: 0-131,738,871
CG density
5mC
K27me3
D
CGC
PMD
chr18:129,396-2,915,124
CG density
5mC FGO
K27me3
FGO
Soma
SHH EN2
Non-CGC
chr18:25,478,491-25,779,258
WNT16
E
Expression of K27me3 regulators
FGO 4C 8C ICM
FGO 4C 16C BI
Out of nucleus
FGO 4C Mo BI
FGO 1C 2C BI
FGO 1C Late 2C ICM
PRC2 complex
EED
SUZ12
EZH2
MTF2
JARID2
Demethylase
KDM6A
KDM6B
PRC1 complex
RING1A
RING1B
KDM2A
KDM2B
-5
5
Log2 (FPKM+0.1)
F
WT vs. Eed mKO FGO
Eed
chr8:107,622,097-108,956,234
5mC
K36me3
K27me3
K27me3
K36me3
Eed
10kb bin
Normalized RPKM
-1
1

Figure S12. H3K27me3 and its relationship with other epigenetic marks in mammalian oocytes. (**A**) Barchart showing the percentages of the genome covered by H3K27me3 (K27me3) in the oocytes among different species. The somatic tissues (Soma) in each species are also similarly analyzed as controls. Arrow indicates the relatively lower genome coverage of H3K27me3 in porcine FGOs. (**B**) Violin plots showing the distribution of CpG density, H3K27me3, H3K4me3 (K4me3), H3K36me2 (K36me2), H3K36me3 (K36me3), PMDs and DNA methylation (5mC) along all chromosomes in the oocytes of all five species. (**C**) UCSC browser views showing H3K27me3 on the whole chromosome 8 in the oocytes of all five species. The DNA methylation and CG density are also shown. (**D**) UCSC browser views showing H3K27me3 in CGCs (left) and non-CGCs (right) in porcine FGOs and somatic cells (Soma). DNA methylation and CG density are also shown. (**E**) Heatmaps showing the expression of H3K27me3 regulators in the oocyte and during the preimplantation development of the five species. Note *EED* and *SUZ12* are expressed but are excluded from nucleus before the morula stage in bovine (*30*) (red box). (**F**) UCSC browser views (top) and heatmap (bottom, 10kb bin) showing the H3K36me3 in wild type (+) and maternal *Eed* knockout (-) mouse FGOs. H3K27me3 in wild type FGOs is also shown.

Figure S13

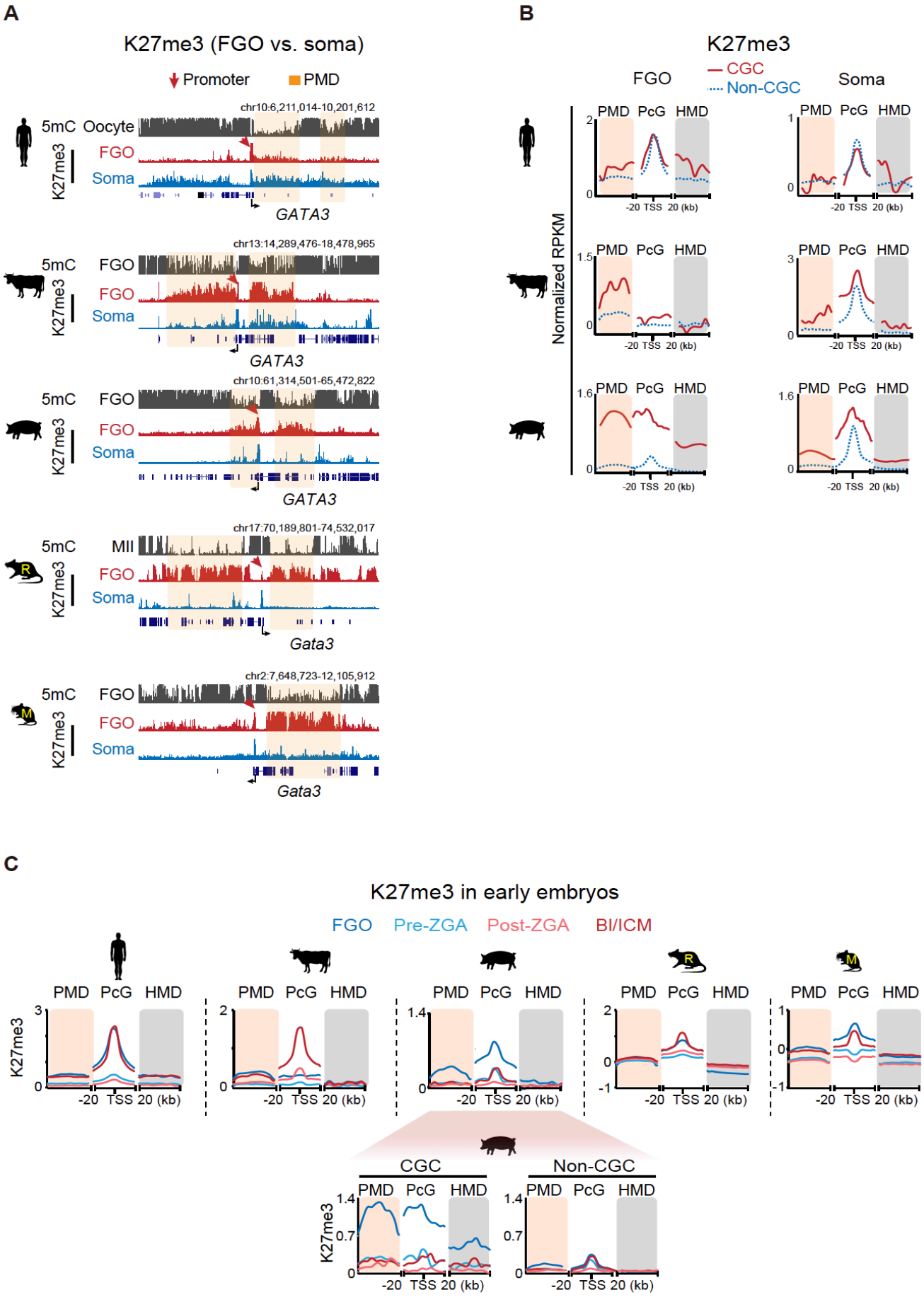
A
K27me3 (FGO vs. soma)
Promoter
PMD
chr10:6,211,014-10,201,612
5mC
Oocyte
K27me3
FGO
Soma
GATA3
chr13:14,289,476-18,478,965
5mC
FGO
K27me3
FGO
Soma
GATA3
chr10:61,314,501-65,472,822
5mC
FGO
K27me3
FGO
Soma
GATA3
chr17:70,189,801-74,532,017
5mC
MII
K27me3
FGO
Soma
Gata3
chr2:7,648,723-12,105,912
5mC
FGO
K27me3
FGO
Soma
Gata3
B
K27me3
FGO
CGC
Non-CGC
Soma
Normalized RPKM
PMD PcG HMD
-20 TSS 20 (kb)
C
K27me3 in early embryos
FGO
Pre-ZGA
Post-ZGA
BI/ICM
K27me3
PMD PcG HMD
-20 TSS 20 (kb)
CGC
Non-CGC

Figure S13. H3K27me3 in mammalian oocytes and preimplantation embryos. (**A**) UCSC genome browser views showing H3K27me3 (K27me3) enrichment around the *Gata3* loci in the FGOs of all five species. DNA methylation in oocytes and H3K27me3 in somatic tissues (Soma) are also shown. (**B**) Metaplots showing H3K27me3 enrichment in PMDs, Polycomb group target gene (PcG) promoters (TSS±20kb) and HMDs in CGC (red) and non-CGC (blue) regions in FGOs (left) and somatic tissues (Soma, right) for human, bovine and porcine. (**C**) Metaplots showing the enrichment of H3K27me3 in PMDs, PcG promoters and HMDs in FGOs and early embryos among the five species (top). CGCs and non-CGCs for porcine are also separately analyzed (bottom). FGO, full-grown oocyte; Bl, blastocyst; ICM, inner cell mass; PMD, partially methylated domain; PcG, Polycomb group gene, HMD, highly methylated domain. CGC, CpG continent.

Figure S14

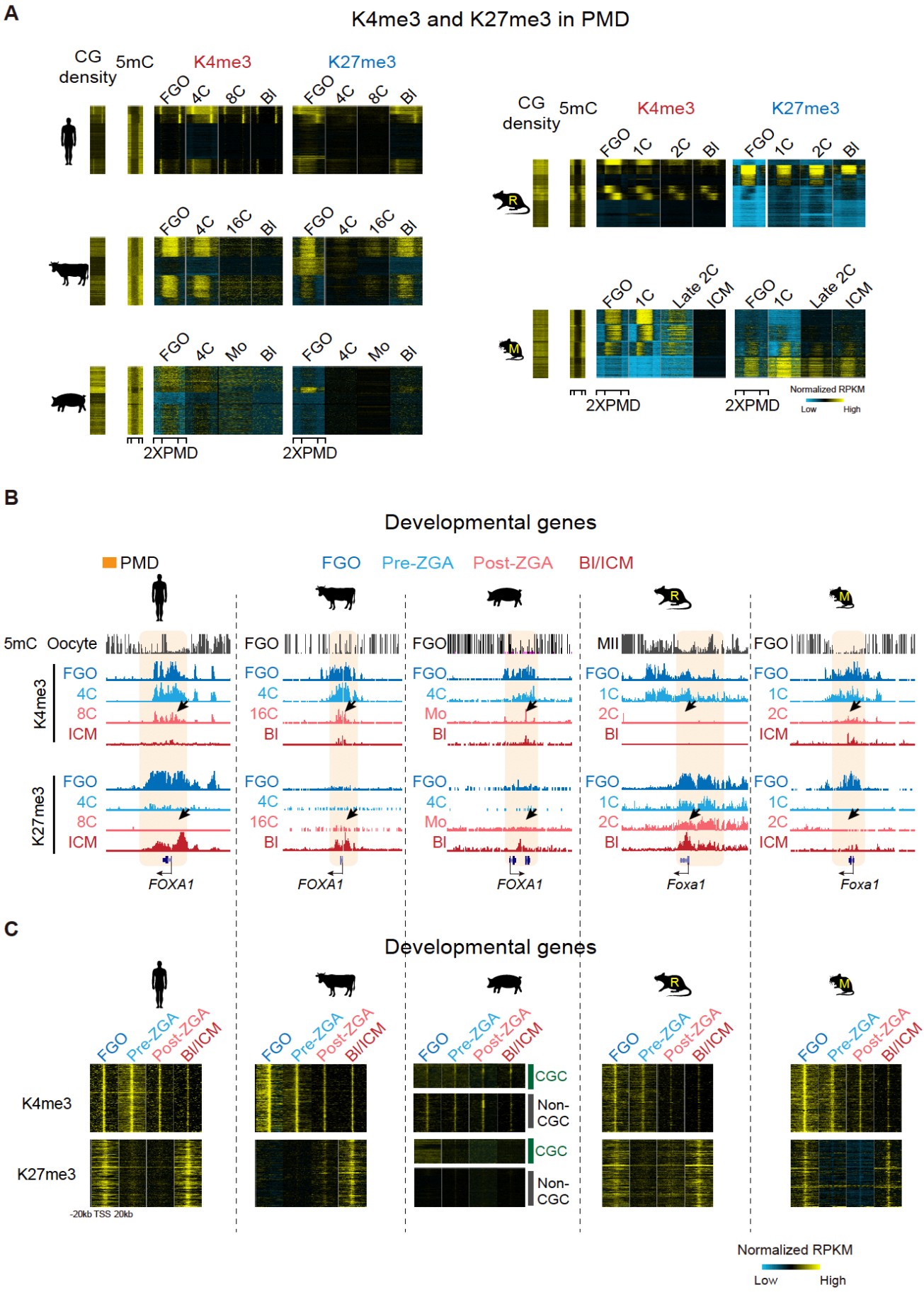
A
K4me3 and K27me3 in PMD
CG density
5mC
K4me3
K27me3
FGO
4C
8C
16C
Mo
BI
1C
2C
Late 2C
ICM
2XPMD
Normalized RPKM
Low
High
B
Developmental genes
PMD
FGO
Pre-ZGA
Post-ZGA
BI/ICM
5mC
Oocyte
MII
K4me3
K27me3
FOXA1
Foxa1
C
Developmental genes
CGC
Non-CGC
-20kb TSS 20kb
Normalized RPKM
Low
High

Figure S14. Dynamics of bivalency at PMD and developmental gene promoters during mammalian preimplantation development. (**A**) Heatmaps showing the enrichment of H3K4me3 and H3K27me7 in the PMDs of mammalian oocytes and their dynamics during mammalian early development. CG density and DNA methylation in PMDs are also shown. FGO, full-grown oocyte; PMD, partially methylated domain; HMD, highly methylated domain; 1C, 1-cell embryo; 2C, late 2-cell embryo; 4C, 4-cell embryo; 8C, 8-cell embryo; 16C, 16-cell embryo; Mo, morula; Bl, Blastocyst; ICM, inner cell mass. (**B**) UCSC genome browser views showing the dynamics of H3K4me3 (K4me3) and H3K27me3 (K27me3) marks at a representative bivalent gene *Foxa1* during preimplantation development of the five species. The arrows indicate the promoter regions at ZGA. The PMD regions are shaded. (**C**) Heatmaps showing the enrichment of H3K4me3 and H3K27me3 marks at bivalent genes from FGO to blastocyst in the five species. Developmental genes are identified in the pluripotent stem cells of each species (Materials and Methods).

Figure S15

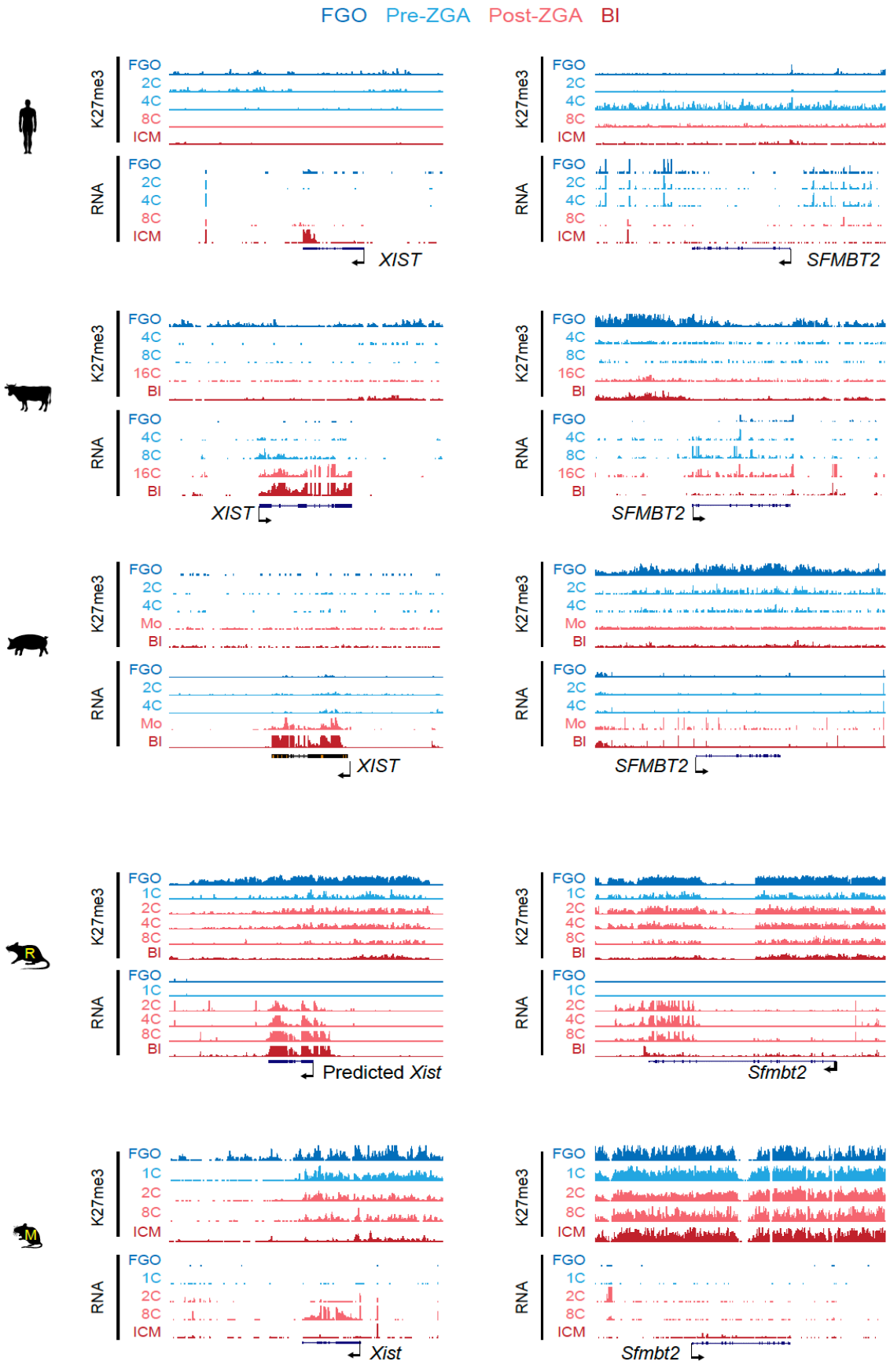
FGO Pre-ZGA Post-ZGA BI
K27me3
RNA
FGO
2C
4C
8C
ICM
XIST
SFMBT2
16C
BI
Mo
1C
Predicted Xist
Sfmbt2
Xist

Figure S15. H3K27me3 and gene expression at the *Xist* and *Sfmbt2* loci during preimplantation development among different species. The UCSC genome browser views showing the enrichment of H3K27me3 (K27me3) and gene expression at *Xist* and *Sfmbt2* loci from FGO to blastocyst in different species. Note the absence of H3K27me3 signals at these two gene loci by ZGA in non-rodents.

Figure S16

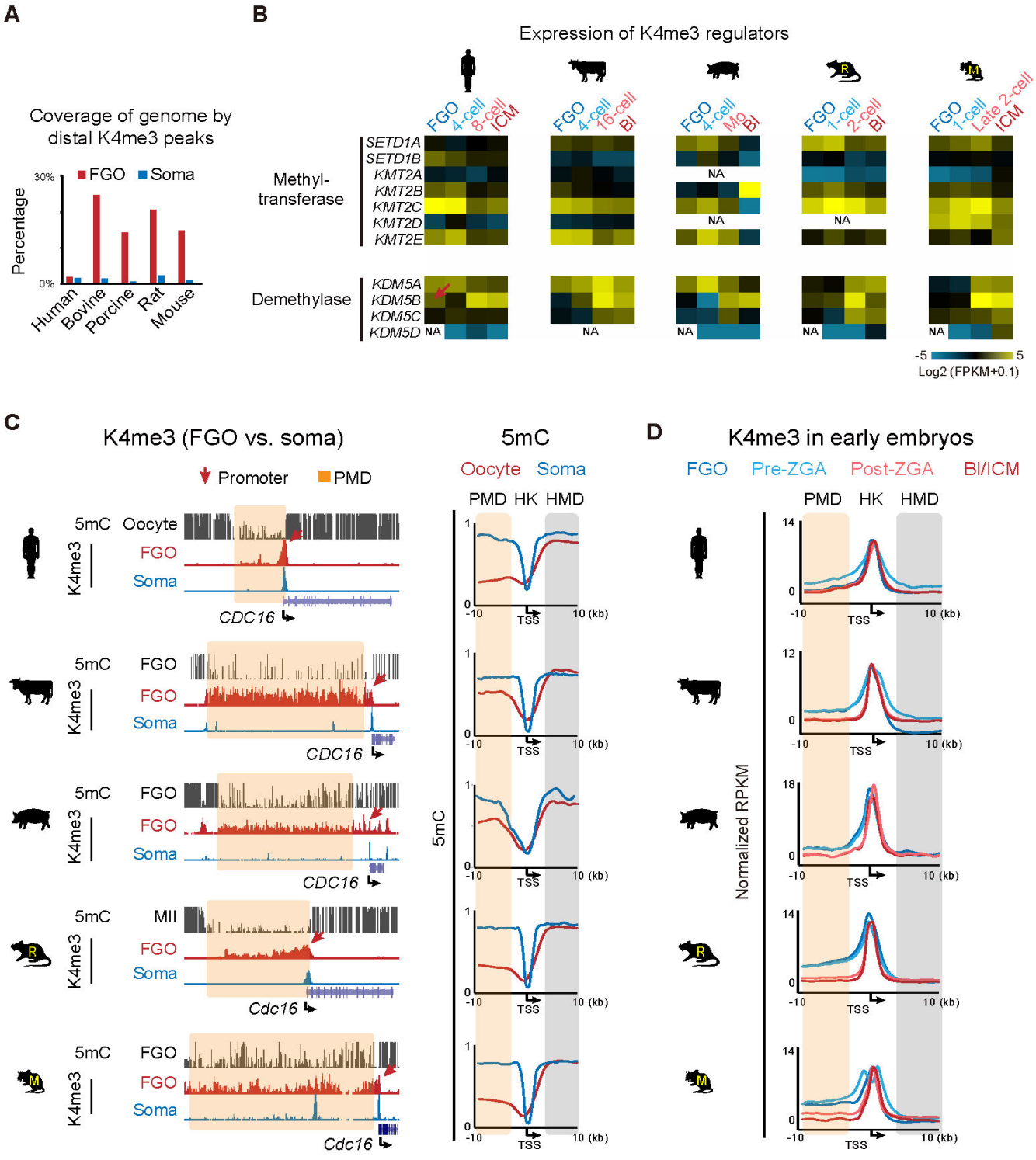
A
Coverage of genome by distal K4me3 peaks
30%
0%
FGO
Soma
Percentage
Human
Bovine
Porcine
Rat
Mouse
B
Expression of K4me3 regulators
FGO 4-cell 8-cell ICM
FGO 4-cell 16-cell Bl
FGO 4-cell Mo Bl
FGO 1-cell 2-cell Bl
FGO 1-cell Late 2-cell ICM
Methyl-transferase
SETD1A
SETD1B
KMT2A
KMT2B
KMT2C
KMT2D
KMT2E
Demethylase
KDM5A
KDM5B
KDM5C
KDM5D
NA
-5
5
Log2 (FPKM+0.1)
C
K4me3 (FGO vs. soma)
Promoter
PMD
5mC
Oocyte
FGO
Soma
MII
K4me3
CDC16
Cdc16
5mC
Oocyte Soma
PMD HK HMD
-10
TSS
10 (kb)
D
K4me3 in early embryos
FGO Pre-ZGA Post-ZGA Bl/ICM
PMD HK HMD
Normalized RPKM

Figure S16. H3K4me3 in mammalian oocytes and preimplantation embryos. (**A**) Barplot showing the genome coverage of distal H3K4me3 (K4me3) peaks in oocyte genomes among different species. Analysis results for the somatic tissues (Soma) in each species are shown as controls. (**B**) Heatmaps showing the expression of H3K4me3 (K4me3) regulators in the oocyte and during the preimplantation development of the five species. Red arrow notes the selective expression of *KDM5B* in the oocytes of human but not other species. (**C**) Left, UCSC genome browser views showing the enrichment of H3K4me3 (K4me3) at the promoter (*Cdc16*) and PMD regions in FGOs of all the five species. H3K4me3 at the promoters and PMD regions are indicated by arrows and shades, respectively. Similar analyses for somatic tissues or cells are shown as controls. Right, metaplots showing the DNA methylation (5mC) at PMDs, promoters, and HMDs around HK genes that have upstream PMDs in oocytes among the five species oocytes (red line). The somatic tissue (blue line) in each species is similarly analyzed as a control. (**D**) Metaplots showing the enrichment of H3K4me3 in PMDs, housekeeping gene promoters (TSS±2.5kb) and HMDs in FGOs and early embryos among the five species.

Figure S17

A

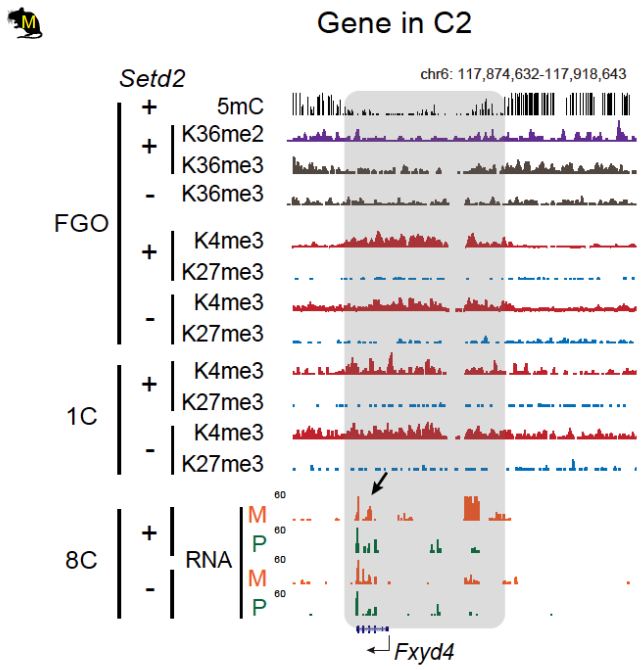

B

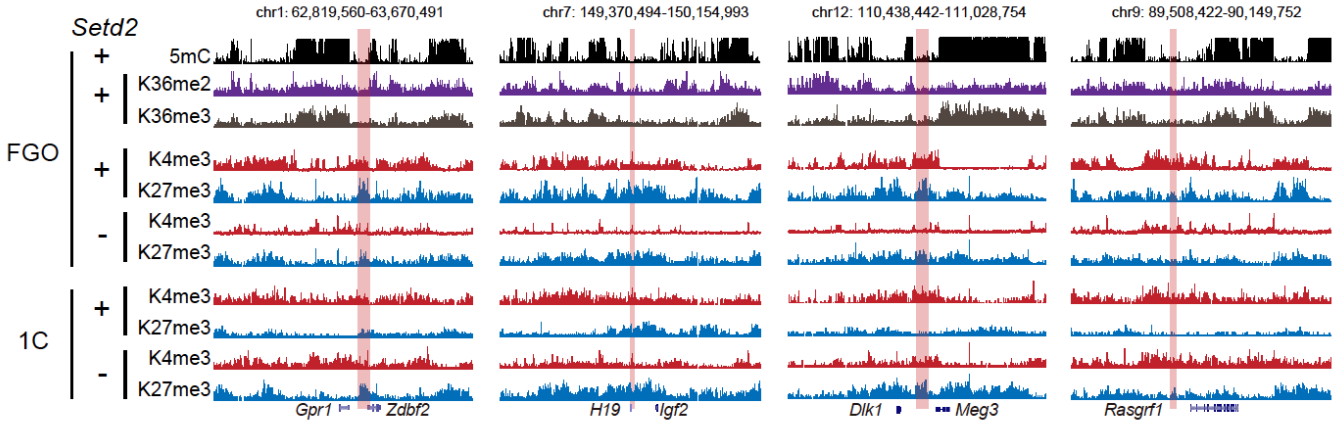

C

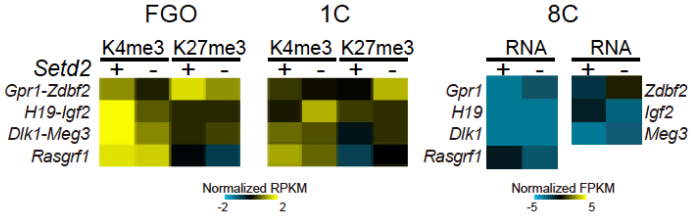

Figure S17. Exclusion of oocyte ncH3K27me3 from ncH3K4me3 domains in rodents. (**A**) The UCSC genome browser view showing the distribution of H3K36me2 (K36me2), H3K36me3 (K36me3), H3K4me3 and H3K27me3 (K27me3), and the maternal and paternal RNA read count signals at a representative gene in cluster 2 (C2, identified in Fig. 6h, where no H3K27me3 invasion is observed) in wild type ("+") and maternal *Setd2* knockout ("-") FGOs. PMD region is shaded. The arrow indicated *Fxyd4* gene locus. (**B** and **C**) The UCSC genome browser views (**B**) and heatmaps (**C,** left and middle) showing the distribution of H3K4me3 (K4me3) and H3K27me3 (K27me3) in the paternal ICRs (shaded) in wild type ("+") and maternal *Setd2* knockout ("-") mouse full-grown oocyte (FGO) and 1-cell (1C) embryo. DNA methylation (5mC), H3K36me2 (K36me2) and H3K36me3 (K36me3) in wild type FGO are shown in the snapshots. Expression of the paternally imprinted genes in wild type and *Setd2* mutant 8C (**C,** right) is shown. *Setd2* mutant 8C embryos are derived from enucleated WT oocytes transferred with *Setd2* mKO chromatin (*9*).

Table S1. (separate file)

Public data used in this study

Table S2. (separate file)

Information for datasets generated in this study

Table S3. (separate file)

Genes located in CGCs in human, bovine and porcine

Table S4. (separate file)

The positions of putative maternal and paternal ICRs in bovine, porcine and rat.

REFERENCES AND NOTES

1. C. D. Allis, T. Jenuwein, The molecular hallmarks of epigenetic control. *Nat. Rev. Genet.* **17**, 487–500 (2016).

2. M. A. Eckersley-Maslin, C. Alda-Catalinas, W. Reik, Dynamics of the epigenetic landscape during the maternal-to-zygotic transition. *Nat. Rev. Mol. Cell Biol.* **19**, 436–450 (2018).

3. M. V. C. Greenberg, D. Bourc'his, The diverse roles of DNA methylation in mammalian development and disease. *Nat. Rev. Mol. Cell Biol.* **20**, 590–607 (2019).

4. T. Suganuma, J. L. Workman, Signals and combinatorial functions of histone modifications. *Annu. Rev. Biochem.* **80**, 473–499 (2011).

5. A. Jambhekar, A. Dhall, Y. Shi, Roles and regulation of histone methylation in animal development. *Nat. Rev. Mol. Cell Biol.* **20**, 625–641 (2019).

6. B. E. Bernstein, T. S. Mikkelsen, X. Xie, M. Kamal, D. J. Huebert, J. Cuff, B. Fry, A. Meissner, M. Wernig, K. Plath, R. Jaenisch, A. Wagschal, R. Feil, S. L. Schreiber, E. S. Lander, A bivalent chromatin structure marks key developmental genes in embryonic stem cells. *Cell* **125**, 315–326 (2006).

7. Y. Li, H. Sasaki, Genomic imprinting in mammals: Its life cycle, molecular mechanisms and reprogramming. *Cell Res.* **21**, 466–473 (2011).

8. K. Shirane, F. Miura, T. Ito, M. C. Lorincz, NSD1-deposited H3K36me2 directs de novo methylation in the mouse male germline and counteracts Polycomb-associated silencing. *Nat. Genet.* **52**, 1088–1098 (2020).

9. Q. Xu, Y. Xiang, Q. Wang, L. Wang, J. Brind'Amour, A. B. Bogutz, Y. Zhang, B. Zhang, G. Yu, W. Xia, Z. Du, C. Huang, J. Ma, H. Zheng, Y. Li, C. Liu, C. L. Walker, E. Jonasch, L. Lefebvre, M. Wu, M. C. Lorincz, W. Li, L. Li, W. Xie, SETD2 regulates the maternal epigenome, genomic imprinting and embryonic development. *Nat. Genet.* **51**, 844–856 (2019).

10. Z. Chen, Y. Zhang, Maternal H3K27me3-dependent autosomal and X chromosome imprinting. *Nat. Rev. Genet.* **21**, 555–571 (2020).

11. Z. Chen, Q. Yin, A. Inoue, C. Zhang, Y. Zhang, Allelic H3K27me3 to allelic DNA methylation switch maintains noncanonical imprinting in extraembryonic cells. *Sci. Adv.* **5**, eaay7246 (2019).

12. C. W. Hanna, R. Perez-Palacios, L. Gahurova, M. Schubert, F. Krueger, L. Biggins, S. Andrews, M. Colome-Tatche, D. Bourc'his, W. Dean, G. Kelsey, Endogenous retroviral insertions drive non-canonical imprinting in extra-embryonic tissues. *Genome Biol.* **20**, 225 (2019).

13. W. Xia, J. Xu, G. Yu, G. Yao, K. Xu, X. Ma, N. Zhang, B. Liu, T. Li, Z. Lin, X. Chen, L. Li, Q. Wang, D. Shi, S. Shi, Y. Zhang, W. Song, H. Jin, L. Hu, Z. Bu, Y. Wang, J. Na, W. Xie, Y. P. Sun, Resetting histone modifications during human parental-to-zygotic transition. *Science* **365**, 353–360 (2019).

14. S. Petropoulos, D. Edsgard, B. Reinius, Q. Deng, S. P. Panula, S. Codeluppi, A. P. Reyes, S. Linnarsson, R. Sandberg, F. Lanner, Single-cell RNA-seq reveals lineage and X chromosome dynamics in human preimplantation embryos. *Cell* **167**, 285 (2016).

15. P. Zhu, H. Guo, Y. Ren, Y. Hou, J. Dong, R. Li, Y. Lian, X. Fan, B. Hu, Y. Gao, X. Wang, Y. Wei, P. Liu, J. Yan, X. Ren, P. Yuan, Y. Yuan, Z. Yan, L. Wen, L. Yan, J. Qiao, F. Tang, Single-cell DNA methylome sequencing of human preimplantation embryos. *Nat. Genet.* **50**, 12–19 (2018).

16. E. Ivanova, S. Canovas, S. Garcia-Martinez, R. Romar, J. S. Lopes, D. Rizos, M. J. Sanchez-Calabuig, F. Krueger, S. Andrews, F. Perez-Sanz, G. Kelsey, P. Coy, DNA methylation changes during preimplantation development reveal inter-species differences and reprogramming events at imprinted genes. *Clin. Epigenetics* **12**, 64 (2020).

17. B. Zhang, H. Zheng, B. Huang, W. Li, Y. Xiang, X. Peng, J. Ming, X. Wu, Y. Zhang, Q. Xu, W. Liu, X. Kou, Y. Zhao, W. He, C. Li, B. Chen, Y. Li, Q. Wang, J. Ma, Q. Yin, K. Kee, A. Meng, S. Gao, F. Xu, J. Na, W. Xie, Allelic reprogramming of the histone modification H3K4me3 in early mammalian development. *Nature* **537**, 553–557 (2016).

18. H. Zheng, B. Huang, B. Zhang, Y. Xiang, Z. Du, Q. Xu, Y. Li, Q. Wang, J. Ma, X. Peng, F. Xu, W. Xie, Resetting epigenetic memory by reprogramming of histone modifications in mammals. *Mol. Cell* **63**, 1066–1079 (2016).

19. J. A. Dahl, I. Jung, H. Aanes, G. D. Greggains, A. Manaf, M. Lerdrup, G. Li, S. Kuan, B. Li, A. Y. Lee, S. Preissl, I. Jermstad, M. H. Haugen, R. Suganthan, M. Bjoras, K. Hansen, K. T. Dalen, P. Fedorcsak, B. Ren, A. Klungland, Broad histone H3K4me3 domains in mouse oocytes modulate maternal-to-zygotic transition. *Nature* **537**, 548–552 (2016).

20. X. Liu, C. Wang, W. Liu, J. Li, C. Li, X. Kou, J. Chen, Y. Zhao, H. Gao, H. Wang, Y. Zhang, Y. Gao, S. Gao, Distinct features of H3K4me3 and H3K27me3 chromatin domains in pre-implantation embryos. *Nature* **537**, 558–562 (2016).

21. C. V. Andreu-Vieyra, R. H. Chen, J. E. Agno, S. Glaser, K. Anastassiadis, A. F. Stewart, M. M. Matzuk, MLL2 is required in oocytes for bulk histone 3 lysine 4 trimethylation and transcriptional silencing. *PLOS Biol.* **8**, e1000453 (2010).

22. W. Zhang, Z. Chen, Q. Yin, D. Zhang, C. Racowsky, Y. Zhang, Maternal-biased H3K27me3 correlates with paternal-specific gene expression in the human morula. *Genes Dev.* **33**, 382–387 (2019).

23. M. M. Halstead, X. Ma, C. Zhou, R. M. Schultz, P. J. Ross, Chromatin remodeling in bovine embryos indicates species-specific regulation of genome activation. *Nat. Commun.* **11**, 4654 (2020).

24. H. Okae, H. Chiba, H. Hiura, H. Hamada, A. Sato, T. Utsunomiya, H. Kikuchi, H. Yoshida, A. Tanaka, M. Suyama, T. Arima, Genome-wide analysis of DNA methylation dynamics during early human development. *PLOS Genet.* **10**, e1004868 (2014).

25. S. A. Smallwood, H. J. Lee, C. Angermueller, F. Krueger, H. Saadeh, J. Peet, S. R. Andrews, O. Stegle, W. Reik, G. Kelsey, Single-cell genome-wide bisulfite sequencing for assessing epigenetic heterogeneity. *Nat. Methods* **11**, 817–820 (2014).

26. J. Brind'Amour, H. Kobayashi, J. Richard Albert, K. Shirane, A. Sakashita, A. Kamio, A. Bogutz, T. Koike, M. M. Karimi, L. Lefebvre, T. Kono, M. C. Lorincz, LTR retrotransposons transcribed in oocytes drive species-specific and heritable changes in DNA methylation. *Nat. Commun.* **9**, 3331 (2018).

27. P. J. Skene, J. G. Henikoff, S. Henikoff, Targeted in situ genome-wide profiling with high efficiency for low cell numbers. *Nat. Protoc.* **13**, 1006–1019 (2018).

28. Y. Zhang, Y. Xiang, Q. Yin, Z. Du, X. Peng, Q. Wang, M. Fidalgo, W. Xia, Y. Li, Z. A. Zhao, W. Zhang, J. Ma, F. Xu, J. Wang, L. Li, W. Xie, Dynamic epigenomic landscapes during early lineage specification in mouse embryos. *Nat. Genet.* **50**, 96–105 (2018).

29. Z. Cao, Y. Li, Z. Chen, H. Wang, M. Zhang, N. Zhou, R. Wu, Y. Ling, F. Fang, N. Li, Y. Zhang, Genome-Wide Dynamic Profiling of Histone Methylation during Nuclear Transfer-Mediated Porcine Somatic Cell Reprogramming. *PLOS ONE* **10**, e0144897 (2015).

30. P. J. Ross, N. P. Ragina, R. M. Rodriguez, A. E. Iager, K. Siripattarapravat, N. Lopez-Corrales, J. B. Cibelli, Polycomb gene expression and histone H3 lysine 27 trimethylation changes during bovine preimplantation development. *Reproduction* **136**, 777–785 (2008).

31. T. Q. Dang-Nguyen, T. Somfai, S. Haraguchi, K. Kikuchi, A. Tajima, Y. Kanai, T. Nagai, In vitro production of porcine embryos: Current status, future perspectives and alternative applications. *Anim. Sci. J.* **82**, 374–382 (2011).

32. A. Piliszek, Z. E. Madeja, Pre-implantation Development of Domestic Animals. *Curr. Top. Dev. Biol.* **128**, 267–294 (2018).

33. N. Irie, S. Kuratani, The developmental hourglass model: A predictor of the basic body plan? *Development* **141**, 4649–4655 (2014).

34. G. Sendzikaite, G. Kelsey, The role and mechanisms of DNA methylation in the oocyte. *Essays Biochem.* **63**, 691–705 (2019).

35. W. Xie, C. L. Barr, A. Kim, F. Yue, A. Y. Lee, J. Eubanks, E. L. Dempster, B. Ren, Base-resolution analyses of sequence and parent-of-origin dependent DNA methylation in the mouse genome. *Cell* **148**, 816–831 (2012).

36. M. Kawahara, Q. Wu, N. Takahashi, S. Morita, K. Yamada, M. Ito, A. C. Ferguson-Smith, T. Kono, High-frequency generation of viable mice from engineered bi-maternal embryos. *Nat. Biotechnol.* **25**, 1045–1050 (2007).

37. Z. Li, H. Wan, G. Feng, L. Wang, Z. He, Y. Wang, X. J. Wang, W. Li, Q. Zhou, B. Hu, Birth of fertile bimaternal offspring following intracytoplasmic injection of parthenogenetic haploid embryonic stem cells. *Cell Res.* **26**, 135–138 (2016).

38. C. Zhong, Z. Xie, Q. Yin, R. Dong, S. Yang, Y. Wu, L. Yang, J. Li, Parthenogenetic haploid embryonic stem cells efficiently support mouse generation by oocyte injection. *Cell Res.* **26**, 131–134 (2016).

39. D. N. Weinberg, S. Papillon-Cavanagh, H. Chen, Y. Yue, X. Chen, K. N. Rajagopalan, C. Horth, J. T. McGuire, X. Xu, H. Nikbakht, A. E. Lemiesz, D. M. Marchione, M. R. Marunde, M. J. Meiners, M. A. Cheek, M. C. Keogh, E. Bareke, A. Djedid, A. S. Harutyunyan, N. Jabado, B. A. Garcia, H. Li, C. D. Allis, J. Majewski, C. Lu, The histone mark H3K36me2 recruits DNMT3A and shapes the intergenic DNA methylation landscape. *Nature* **573**, 281–286 (2019).

40. S. Bhattacharya, J. L. Workman, Regulation of SETD2 stability is important for the fidelity of H3K36me3 deposition. *Epigenetics Chromatin* **13**, (2020), 40.

41. W. Yuan, M. Xu, C. Huang, N. Liu, S. Chen, B. Zhu, H3K36 methylation antagonizes PRC2-mediated H3K27 methylation. *J. Biol. Chem.* **286**, 7983–7989 (2011).

42. F. W. Schmitges, A. B. Prusty, M. Faty, A. Stützer, G. M. Lingaraju, J. Aiwazian, R. Sack, D. Hess, L. Li, S. L. Zhou, R. D. Bunker, U. Wirth, T. Bouwmeester, A. Bauer, N. Ly-Hartig, K. H. Zhao, H. M. Chan, J. Gu, H. Gut, W. Fischle, J. Müller, N. H. Thomä, Histone methylation by PRC2 is inhibited by active chromatin marks. *Mol. Cell* **42**, 330–341 (2011).

43. N. P. Blackledge, N. R. Rose, R. J. Klose, Targeting Polycomb systems to regulate gene expression: Modifications to a complex story. *Nat. Rev. Mol. Cell Biol.* **16**, 643–649 (2015).

44. W. Xia, W. Xie, Rebooting the epigenomes during mammalian early embryogenesis. *Stem Cell Reports* **15**, 1158–1175 (2020).

45. N. Wake, N. Takagi, M. Sasaki, Non-random inactivation of X chromosome in the rat yolk sac. *Nature* **262**, 580–581 (1976).

46. B. Min, J. S. Park, K. Jeon, Y.-K. Kang, Characterization of X-chromosome gene expression in bovine blastocysts derived by in vitro fertilization and somatic cell nuclear transfer. *Front. Genet.* **8**, 42 (2017).

47. D. Yu, X. Du, J. Wang, L. Chen, Y. Wang, H. Xu, Y. Zhao, S. Zhao, Y. Pang, Y. Liu, H. Hao, X. Zhao, W. Du, Y. Dai, N. Li, S. Wu, H. Zhu, No imprinted *XIST* expression in pigs: Biallelic *XIST* expression in early embryos and random X inactivation in placentas. *Cell. Mol. Life Sci.* **76**, 4525–4538 (2019).

48. J. Huang, H. Zhang, X. Wang, K. B. Dobbs, J. Yao, G. Qin, K. Whitworth, E. M. Walters, R. S. Prather, J. Zhao, Impairment of preimplantation porcine embryo development by histone demethylase KDM5B knockdown through disturbance of bivalent H3K4me3-H3K27me3 modifications. *Biol. Reprod.* **92**, 72 (2015).

49. Y. Xiang, Y. Zhang, Q. Xu, C. Zhou, B. Liu, Z. Du, K. Zhang, B. Zhang, X. Wang, S. Gayen, L. Liu, Y. Wang, Y. Li, Q. Wang, S. Kalantry, L. Li, W. Xie, Epigenomic analysis of gastrulation identifies a unique chromatin state for primed pluripotency. *Nat. Genet.* **52**, 95–105 (2020).

50. G. Yang, L. Zhang, W. Liu, Z. Qiao, S. Shen, Q. Zhu, R. Gao, M. Wang, M. Wang, C. Li, M. Liu, J. Sun, L. Wang, W. Liu, X. Cui, K. Zhao, R. Zang, M. Chen, Z. Liang, L. Wang, X. Kou, Y. Zhao, H. Wang, Y. Wang, S. Gao, J. Chen, C. Jiang, Dux-mediated corrections of aberrant H3K9ac during 2-cell genome activation optimize efficiency of somatic cell nuclear transfer. *Cell Stem Cell* **28**, 150–163.e5 (2021).

51. A. Inoue, L. Jiang, F. Lu, T. Suzuki, Y. Zhang, Maternal H3K27me3 controls DNA methylation-independent imprinting. *Nature* **547**, 419–424 (2017).

52. A. Inoue, Z. Chen, Q. Yin, Y. Zhang, Maternal *Eed* knockout causes loss of H3K27me3 imprinting and random X inactivation in the extraembryonic cells. *Genes Dev.* **32**, 1525–1536 (2018).

53. A. M. Deaton, A. Bird, CpG islands and the regulation of transcription. *Genes Dev.* **25**, 1010–1022 (2011).

54. S. K. T. Ooi, C. Qiu, E. Bernstein, K. Li, D. Jia, Z. Yang, H. Erdjument-Bromage, P. Tempst, S.-P. Lin, C. D. Allis, X. Cheng, T. H. Bestor, DNMT3L connects unmethylated lysine 4 of histone H3 to de novo methylation of DNA. *Nature* **448**, 714–717 (2007).

55. A. B. Brinkman, H. Gu, S. J. Bartels, Y. Zhang, F. Matarese, F. Simmer, H. Marks, C. Bock, A. Gnirke, A. Meissner, H. G. Stunnenberg, Sequential ChIP-bisulfite sequencing enables direct genome-scale investigation of chromatin and DNA methylation cross-talk. *Genome Res.* **22**, 1128–1138 (2012).

56. T. Moore, D. Haig, Genomic imprinting in mammalian development: A parental tug-of-war. *Trends Genet.* **7**, 45–49 (1991).

57. Y. W. Cho, T. Hong, S. Hong, H. Guo, H. Yu, D. Kim, T. Guszczynski, G. R. Dressler, T. D. Copeland, M. Kalkum, K. Ge, PTIP associates with MLL3- and MLL4-containing histone H3 lysine 4 methyltransferase complex. *J. Biol. Chem.* **282**, 20395–20406 (2007).

58. S. Picelli, O. R. Faridani, A. K. Bjorklund, G. Winberg, S. Sagasser, R. Sandberg, Full-length RNA-seq from single cells using Smart-seq2. *Nat. Protoc.* **9**, 171–181 (2014).

59. X. Peng, J. Wu, R. Brunmeir, S. Y. Kim, Q. Zhang, C. Ding, W. Han, W. Xie, F. Xu, TELP, a sensitive and versatile library construction method for next-generation sequencing. *Nucleic Acids Res.* **43**, e35 (2015).

60. B. Langmead, S. L. Salzberg, Fast gapped-read alignment with Bowtie 2. *Nat. Methods* **9**, 357–359 (2012).

61. C. Trapnell, L. Pachter, S. L. Salzberg, TopHat: Discovering splice junctions with RNA-Seq. *Bioinformatics* **25**, 1105–1111 (2009).

62. C. Trapnell, A. Roberts, L. Goff, G. Pertea, D. Kim, D. R. Kelley, H. Pimentel, S. L. Salzberg, J. L. Rinn, L. Pachter, Differential gene and transcript expression analysis of RNA-seq experiments with TopHat and Cufflinks. *Nat. Protoc.* **7**, 562–578 (2012).

63. M. Martin, Cutadapt removes adapter sequences from high-throughput sequencing reads. *EMBnet J.* **17**, 10 (2011).

64. F. Krueger, S. R. Andrews, Bismark: A flexible aligner and methylation caller for Bisulfite-Seq applications. *Bioinformatics* **27**, 1571–1572 (2011).

65. E. Becht, L. McInnes, J. Healy, C. A. Dutertre, I. W. H. Kwok, L. G. Ng, F. Ginhoux, E. W. Newell, Dimensionality reduction for visualizing single-cell data using UMAP. *Nat. Biotechnol.* **37**, 38–44 (2019).

66. S. Durinck, Y. Moreau, A. Kasprzyk, S. Davis, B. De Moor, A. Brazma, W. Huber, BioMart and Bioconductor: A powerful link between biological databases and microarray data analysis. *Bioinformatics* **21**, 3439–3440 (2005).

67. B. J. Lesch, S. J. Silber, J. R. McCarrey, D. C. Page, Parallel evolution of male germline epigenetic poising and somatic development in animals. *Nat. Genet.* **48**, 888–894 (2016).

68. R. Lister, M. Pelizzola, R. H. Dowen, R. D. Hawkins, G. Hon, J. Tonti-Filippini, J. R. Nery, L. Lee, Z. Ye, Q. M. Ngo, L. Edsall, J. Antosiewicz-Bourget, R. Stewart, V. Ruotti, A. H. Millar, J. A. Thomson, B. Ren, J. R. Ecker, Human DNA methylomes at base resolution show widespread epigenomic differences. *Nature* **462**, 315–322 (2009).

69. Y. S. Bogliotti, J. Wu, M. Vilarino, D. Okamura, D. A. Soto, C. Zhong, M. Sakurai, R. V. Sampaio, K. Suzuki, J. C. Izpisua Belmonte, P. J. Ross, Efficient derivation of stable primed pluripotent embryonic stem cells from bovine blastocysts. *Proc. Natl. Acad. Sci. U.S.A.* **115**, 2090–2095 (2018).

70. S. Xiao, D. Xie, X. Cao, P. Yu, X. Xing, C. C. Chen, M. Musselman, M. Xie, F. D. West, H. A. Lewin, T. Wang, S. Zhong, Comparative epigenomic annotation of regulatory DNA. *Cell* **149**, 1381–1392 (2012).

71. G. Dennis Jr., B. T. Sherman, D. A. Hosack, J. Yang, W. Gao, H. C. Lane, R. A. Lempicki, DAVID: Database for Annotation, Visualization, and Integrated Discovery. *Genome Biol.* **4**, P3 (2003).

72. J. Wu, B. Huang, H. Chen, Q. Yin, Y. Liu, Y. Xiang, B. Zhang, B. Liu, Q. Wang, W. Xia, W. Li, Y. Li, J. Ma, X. Peng, H. Zheng, J. Ming, W. Zhang, J. Zhang, G. Tian, F. Xu, Z. Chang, J. Na, X. Yang, W. Xie, The landscape of accessible chromatin in mammalian preimplantation embryos. *Nature* **534**, 652–657 (2016).

3. ENCODE Project Consortium, An integrated encyclopedia of DNA elements in the human genome. *Nature* **489**, 57–74 (2012).

74. Y. Zhou, S. L. Liu, Y. Hu, L. Z. Fang, Y. H. Gao, H. Xia, S. G. Schroeder, B. D. Rosen, E. E. Connor, C. J. Li, R. L. Baldwin, J. B. Cole, C. P. Van Tassell, L. G. Yang, L. Ma, G. E. Liu, Comparative whole genome DNA methylation profiling across cattle tissues reveals global and tissue-specific methylation patterns. *BMC Biol.* **18**, 85 (2020).

75. M. D. Johnson, M. Mueller, M. Adamowicz-Brice, M. J. Collins, P. Gellert, K. Maratou, P. K. Srivastava, M. Rotival, S. Butt, L. Game, S. S. Atanur, N. Silver, P. J. Norsworthy, S. R. Langley, E. Petretto, M. Pravenec, T. J. Aitman, Genetic analysis of the cardiac methylome at single nucleotide resolution in a model of human cardiovascular disease. *PLOS Genet.* **10**, e1004813 (2014).

76. G. C. Hon, N. Rajagopal, Y. Shen, D. F. McCleary, F. Yue, M. D. Dang, B. Ren, Epigenetic memory at embryonic enhancers identified in DNA methylation maps from adult mouse tissues. *Nat. Genet.* **45**, 1198–1206 (2013).

77. Y. Shen, F. Yue, D. F. McCleary, Z. Ye, L. Edsall, S. Kuan, U. Wagner, J. Dixon, L. Lee, V. V. Lobanenkov, B. Ren, A map of the cis-regulatory sequences in the mouse genome. *Nature* **488**, 116–120 (2012).

78. Y. Yang, X. Fan, J. Yan, M. Chen, M. Zhu, Y. Tang, S. Liu, Z. Tang, A comprehensive epigenome atlas reveals DNA methylation regulating skeletal muscle development. *Nucleic Acids Res.* **49**, 1313–1329 (2021).

79. J. E. Duan, Z. C. Jiang, F. Alqahtani, I. Mandoiu, H. Dong, X. Zheng, S. L. Marjani, J. Chen, X. C. Tian, Methylome dynamics of bovine gametes and in vivo early embryos. *Front. Genet.* **10**, 512 (2019).

80. Z. Du, H. Zheng, Y. K. Kawamura, K. Zhang, J. Gassler, S. Powell, Q. Xu, Z. Lin, K. Xu, Q. Zhou, E. A. Ozonov, N. Véron, B. Huang, L. Li, G. Yu, L. Liu, W. K. A. Yeung, P. Wang, L. Chang, Q. Wang, A. He, Y. Sun, J. Na, Q. Sun, H. Sasaki, K. Tachibana, A. H. F. M. Peters, W. Xie, Polycomb group proteins regulate chromatin architecture in mouse oocytes and early embryos. *Mol. Cell* **77**, 825–839.e7 (2020).

81. L. Wang, J. Zhang, J. Duan, X. Gao, W. Zhu, X. Lu, L. Yang, J. Zhang, G. Li, W. Ci, W. Li, Q. Zhou, N. Aluru, F. Tang, C. He, X. Huang, J. Liu, Programming and inheritance of parental DNA methylomes in mammals. *Cell* **157**, 979–991 (2014).